University of Stavanger

FACULTY OF SCIENCE AND TECHNOLOGY

MASTER'S THESIS

Study programme/specialisation: **Petroleum Engineering Master /** ***(Reservoir Specialisation)***	**Spring semester, 2018** **Open**
Author: **Nataliya Linev´yuk**	…… (signature of author)
Supervisor: **Pål Østebø Andersen**	
Title of master's thesis: **Simulation study of co-current spontaneous imbibition**	
Credits (ECTS): 30	
Keywords: • Spontaneous Imbibition • Co-Current • Counter-Current • Two-Ends Open • IORCoreSim • Capillary Back pressure • Simulation study	Number of pages: 60 + supplemental material/other:1 Stavanger, 27/08/2018

Abstract

Spontaneous imbibition is the main driving mechanism for obtaining high recovery from the naturally fractured reservoirs with low permeable matrix.

The present thesis presents the results of a simulation study of one-dimensional, co-current spontaneous imbibition in a strongly water-wet sample. Experimental data used for this work was taken from Haugen et al. (2014, 2015). The circumstances of the experiments were characterized by one end face of the core to be open to brine (an inlet) and the other end face to be open to oil (an outlet). Under this Two-Ends-Open (TEO) boundary condition both co- and counter-current flow can take place at the same time, in other words, the inlet can be produced counter-currently and the outlet - co-currently.

The simulation program IORCoreSim was used in this thesis to model the system. The water-oil flow was developed by using Corey relative permeability type and J-function capillary pressure correlation. The experiments were matched by establishing relative permeability and capillary pressure curves. After the match was obtained, the saturation functions were used to perform the sensitivity analysis. It was done by varying several parameters: mobility ratio by holding one of viscosities fixed while changing the other, then both viscosities at fixed mobility ratio, and furthermore capillary back pressure. The last two cases were performed at M=0.01 and M=11.

With increased oil viscosity at fixed water viscosity, the imbibition rate was observed to be lower with decreasing co-current recovery, while counter-current recovery was increased. The breakthrough time was delayed. With increased water viscosity at fixed oil viscosity, the trends for inlet and outlet recovery were similar with increased imbibition time. The breakthrough time was also delayed.

For fixed mobility ratio with varying both viscosities, the trend showed that increased viscosity ratio has no impact on total production and co-current recovery was reduced as M increased whereas counter-current increased.

The capillary back pressure influenced essentially the system at M=11 when compared with M=0.01. Counter-current recovery decreased with increasing capillary back pressure at values beyond the threshold capillary pressure.

Acknowledgement

I can describe writing of my Master thesis as an adventure with a good and exciting start that ended up being the toughest times of my studies at UiS. I faced unexpected difficulties in my life both private and related studies that turned my writing into a big challenge. Despite all this, I collected myself and tried my best.

Pål Ø. Andersen, I would like to express my sincere gratitude and appreciation for your guidance throughout the writing process, your advice and availability. Your days and nights spent at UiS will be paid off in the future and I wish you to become one of the most productive researchers of Norway.

I am also thankful to all of those with whom I have had the pleasure to work during my writing. Arild Lohne, thank you for your explanations and availability, now I know that water can be both "smart" and "stupid". Oddbjørn Nødland, thanks for your time, wish you success with your PhD thesis. Skule Strand, thanks for your positive attitude and smiles during our meetings and willing to help. Anita Malde and Rebecca Adele Esaiassen, thank you both very much for your help.

I also would like to express my special thanks of gratitude to Kristine Femsteinevik who supported me so much during this difficult time.

I want to acknowledge everyone who played a role in my academic accomplishments, especially Papi Ninga, Remi Erempagamo, Kitty Shearer and Dennis Ginn.

Isaac, I cannot thank you enough for everything. You are nothing less than a blessing from God. All is well!!!

My lovely family, I know you are proud of me and my accomplishments, thanks for support and love.

May God bless everyone with all the success and happiness in life.

Table of Contents

List of Tables

List of Figures

Abbreviations

μ_o	Oil viscosity
μ_w	Water viscosity
1D	One-Dimensional
COBR	Crude Oil/Brine/Rock
COCSI	Co-Current Spontaneous Imbibition
COUCSI	Counter-Current Spontaneous Imbibition
k_r	Relative Permeability
M	Mobility ratio
NW	Non-Wetting
P_c	Capillary Pressure
SI	Spontaneous Imbibition
TEO	Two-Ends Open
TEOFSI	Two-ends Open Free Spontaneous Imbibition
W	Wetting

1 INTRODUCTION

This chapter describes the motivation behind the simulation study of co-current spontaneous imbibition. It includes a background section which starts from a broad perspective and challenges of naturally fractured reservoirs and follows by the motivation for the essence of co-current spontaneous imbibition in carbonates. The specific goals of the present study are also presented herein.

1.1 Background

In a fractured reservoir, the matrix blocks that contain most of the oil are bounded by a fracture network with higher permeability than that of the matrix. It leads to injected fluids channelling through the fracture system readily and limiting their entry into the matrix structure to displace oil towards the producing wells. This causes early water-breakthrough and minimizes the efficiency of the recovery process by waterflooding. In the 1950s, Brownscombe et al., (1952) studied the Spraberry formation and noted that conventional recovery by gas or water injection would not be suitable due to the high degree of fracturing, but substantial self-uptake of water was observed to take place. In the years that followed, their findings initiated the investigation of water imbibition displacement processes with reports in the literature and field observations confirming spontaneous imbibition (SI) of the injected fluid as a chief mechanism to yield high recovery in fractured rocks (Wade, 1974; Austad et al., 1997; Akin et al., 1998; Zhou et al., 2000). Up to 1992 Zhou et al., (2000) compiled a comprehensive summary of some experimental studies geared towards the study of imbibition. Today, this phenomenon, which describes the spontaneous uptake of injected fluid continues to receive attention from other researchers that study it in order to better understand the underlying principles governing it.

Capillary pressure is regarded as the main driving force for SI, since imbibition is driven by surface energy. However, the degree of its impact and the extent to which oil is displaced from the matrix of the fractured reservoirs depends on the Crude Oil/Brine/Rock (COBR) interactions, which depend on wetting and two-phase flow, and is governed by the inter-related complexities of the chemistry and physical properties of all three COBR components, the fracture geometry and pore structure of the rock (Morrow et al., 2001). In a two-phase oil/water fluid system, positive capillary pressure favours the SI of the wetting fluid into the porous medium. Seeing as oil is the target fluid for production, SI of injected brine is the desired goal and thus water-wetness of the matrix is imperative to yield high recovery (Anderson, 1987; Austad & Milter, 1997; Frida, 1998). A schematic representation of water imbibing into a fractured oil-saturated rock is shown in Figure 1.1

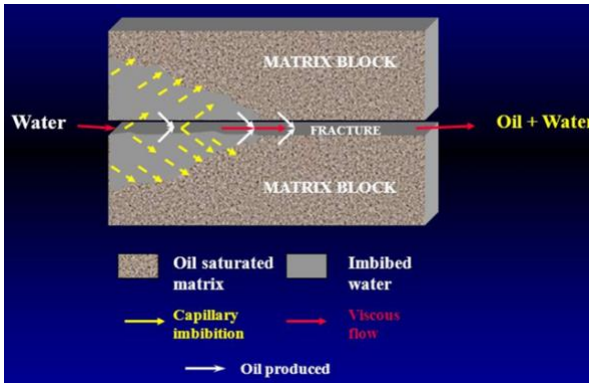

Figure 1.1: *Schematic representation of displacement process in fractured medium (Frida, 1998).*

Co-Current Spontaneous Imbibition (COCSI) and Counter-Current Spontaneous Imbibition (COUCSI) are the two spontaneous imbibition types that can arise, based on the flow direction of the wetting and non-wetting phases (Mattax et al., 1962; Pooladi-Darvish & Firoozabadi, 2000; Karpyn et al., 2009; Standnes, 2004; Cai et al., 2010). For counter-current imbibition, the wetting and non-wetting phase flow through the same face in opposite direction whilst for co-current imbibition, the wetting and non-wetting phase flow through the different faces in the same direction. A simplistic representation of these two processes are illustrated in Figure 2.

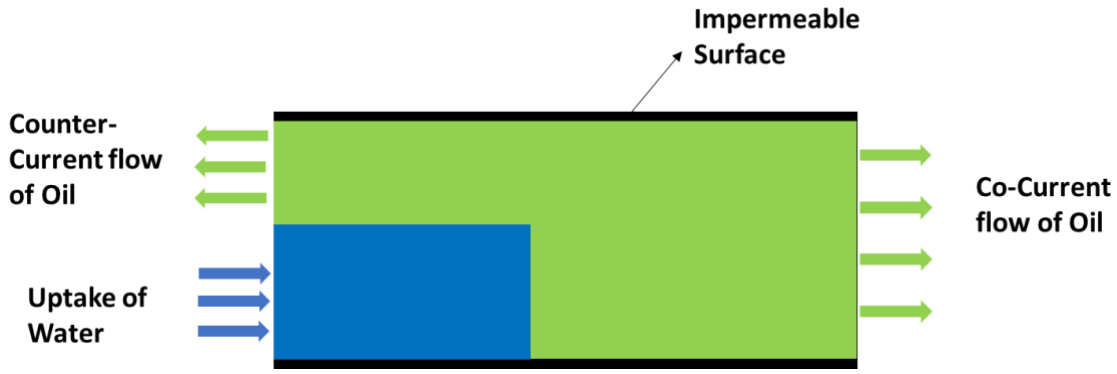

Figure 1.2: *Illustration of Co-current and Counter-current SI (modified from Haugen, et al., (2014)).*

It is clearly noticed from Figure 1.2 that the specific mechanism that will dominate, depends on the sections of the sample where impermeable boundaries exist. Hamidpour et al., (2015) points out that COUCSI will occur when all the permeable faces of a matrix block are brought into contact with a wetting phase, whilst COCSI occurs when only a portion of the permeable surfaces is in contact with wetting phase and the remaining permeable surfaces are covered by nonwetting phase. On a more realistic field-scale environment, the prevailing type of SI during water drive will be dictated by the degree of fracturing (Qasem et al., 2008), strength of gravitational forces (Schechter et al., 1994) and the degree of capillary forces and magnitude of capillary to gravity forces (Bourbiaux, 2009). It is asserted by Karpyn et al., (2009) that both co- and counter-current SI may coexist during waterfloods in fractured reservoirs, but the flow of each phase is different in the two SI modes. The flow mode will depend on which phases surround the block. Pooladi-Darvish & Firoozabadi, (2000) pointed out the crucial influence of wetting phase injection rate into the fracture network of the rock and Standnes (2004) through experimental study of the impact of different boundary conditions on each SI process revealed that the relative position of matrix blocks with respect to the injection well or aquifer (source of non-wetting fluid) will also play a role in determining the prevailing SI process. If the block is surrounded symmetrically by water, COUCSI dominates. Whereas, if the block has water on one side and oil on the other, COCSI can dominate. It is noteworthy that countercurrent production at the side covered by water can still occur during COCSI. Different authors have reported different magnitudes of contribution to recovery from each SI type, with many authors (Morrow & Mason, 2001; Schmid & Geiger, 2011; Mason & Morrow, 2013) originally focusing on COUCSI as the most prevailing process. It is worthy of note, however, that as the two processes are dependent on several factors as outlined, above, the dominance of any single mode will be dictated by the dominant factors imposed on the rock sample.

Bourbiaux & Kalaydjian (1990) performed an experimental study on co- and counter-current flows in natural porous medium and reported the ultimate recovery and rate of co-current oil production to be much faster than for counter-current production. Also, experimental and numerical work of COCSI and COUCSI conducted by Pooladi-Darvish & Firoozabadi, (2000) on stacks of matrix blocks of Berea and Kansas chalk indicated that co-current flow can be faster and attain higher ultimate recovery than for dominant counter-current flows. Similar results to these findings were reported by other authors, (Standnes, 2004; Karimaie et al., 2006; Unsal et al., 2009; Fernø et al., 2014; Hamidpour et al., 2015).

Most of the aforementioned results were made by considering strongly water-wet rock samples. However, as reported by Treiber et al., (1972) and further emphasized by Chilingar et al., (1983), carbonates are generally fractured and exhibit mix-or oil-wet tendencies. Owing to this huge potential for improved recovery from these formations, some authors (Austad et al., 1998; Gupta & Mohanty, 2010) have also given attention to SI under these wetting conditions. Also, since water-wetness is the preferred state for higher SI influence, the methods of wettability alteration in carbonates to facilitate oil recovery is also an active area of research and findings of such methods are covered in the literature (Austad & Milter, 1997; Strand et al., 2007; Puntervold et al., 2016).

Laboratory imbibition experiments, just like several other experimental investigations usually span over long periods of time, and usually performed on rock samples that cover a minute fraction of the vast reservoir framework. Thus, analytical and numerical studies are usually conducted in a bid to fit mathematical models to mimic the result of experimental findings. This way, the acting parameters can be varied to investigate their effect and modified to upscale laboratory imbibition experiments to field-scale dimensions. These numerical models are the backbone of simulation tools used to study SI processes on the large scale. Various boundary conditions (BC) have been applied in the experimental investigation of SI; All Faces Open (AFO) (Mason et al., 2009; Fernø et al., 2014), One End Open (OEO) (Akin et al., 1998; Li et al., 2003), Two Ends Closed (TEC) (Fischer et al., 2006), Two Ends Open (TEO) (Bourbiaux & Kalaydjian, 1990; Yoldiz et al., 2006; Mason et al., 2010) and a special form of the TEO boundary condition, TEOFSI, introduced by (Haugen et al., 2014) where one end face of the core is exposed to brine and the other end face is exposed to oil. This new BC has further been explored by other authors (Haugen et al., 2015; Hamidpour et al., 2015; Meng et al., 2017)

Regarding numerical models, In the 1960s, Handy (1960) successfully developed an analytical model to calculate the imbibition rates of water into a porous media. He described a 1D water-gas COCSI based on the assumption of piston-like displacement and showed that gas recovery was varying linearly with square root of time. Several other authors (McWhorter et al., 1990; Li et al., 2006; Fischer et al., 2006; Li, 2007; Bourbiaux, 2009; Schmid et al., 2011; Andersen et al., 2013; Haugen et al., 2014) have contributed to enhancing the model, proposing new and improved schemes and incorporating more complexities to better define the complexity of the process. A recent contribution to this learning published by Standnes & Andersen, (2017) introduced a new dimensionless time as likened to the expressions of Ma et al., (1997), and Mason et al., (2010). The new parameter which allows for better accuracy for upscaling laboratory COUCSI experiments that cover a wide range of viscosities incorporates the curvature and end-point of the relative permeability functions as well as fluid-fluid interaction parameters and deemed universally valid, in principle, for estimating fluid mobilities at counter-current flow for all fluid viscosities and all relative permeability shapes.

These mathematical models, however, do have limitations as to their abilities to capture all the factors dictating the output of SI processes, especially since the porous media is hugely complex with characteristics that are not yet fully understood. There is therefore a continual need to study both COCSI and COUCSI in the laboratory to progressively understand the effects of different factors influencing the process.

It is important to note, also, that experiments performed in a particular lab is hardly reproducible in a different lab when standard boundary conditions are not complied with during the process. A typical example is the 1D experimental work performed by Hatiboglu & Babadagli, (2010) regarding water-air co- and counter- current SI tests on Berea sandstone at two different temperatures. They observed that at low temperature the displacement rate and final recovery by the COCSI were faster and higher than the COUCSI counterpart. However, at the higher temperature even though the ultimate recovery by the COCSI was higher, the COUCSI displacement was faster than the COCSI test. They also reported doing water-oil COCSI tests. However, as later pointed out by Hamidpour et al., (2015), both boundary conditions used were not in accordance with common pure COCSI boundary conditions. In one case, water was in contact with the bottom face of the oil saturated porous medium which was free to atmosphere through the top face. In another case, both bottom and top faces of the 1D medium were in contact with water. As mentioned in the previous text, dominant COCSI occurs when only a portion of the permeable surfaces is in contact with wetting phase and the remaining permeable surfaces are covered by nonwetting phase.

Haugen et al., (2014) conducted 1D water-oil COCSI experiments on consolidated Portland Chalk and Bentheimer Sandstone with setup like Figure 1.2 (TEOFSI). Oil production by counter-current flow only occurred in the very early stage of imbibition, and for their nine tests, an average of 96% of total recovery was produced by COCSI. They further used sensitivity analysis to discuss the impact of viscosity ratio on the production rates and concluded that counter-current imbibition progresses for almost the entire imbibition period when the oil viscosity is increased relative to the water viscosity. They noted, also, that increasing the fluid viscosities slowed production. They also showed that the relative permeability to oil behind the front increased as the oil was made more viscous. Meng et al., (2015) studied COCSI by applying the TEOFSI on unconsolidated glass bead and quartz sand porous media to analyze the impact of increasing non-wetting phase viscosity and reported that the magnitude of oil entrapment and relative permeability to brine behind the imbibition front had no significant changes when glass beads are used. However, the magnitude of entrapment increases, and the relative permeability decreases enormously with increase in the viscosity when quartz sand packs are used. Meng et al., (2016) applied the same system of porous media to investigate the effect of wetting phase viscosity on COCSI and found that the residual oil saturation was independent of the wetting-phase viscosity for both systems but rather on the pore geometry and pore size distribution of the porous media. They also noted rapid decrease in the rate of oil production by COCSI with increasing wetting phase viscosity.

The surveyed literature suggests that that the parameters controlling imbibition into oil-filled cores are complex and elusive to ascertain and further investigation into the impact of any single factor deemed relevant in the dynamic displacement aspects of the SI process is vital and could contribute to the current knowledge of the subject matter.

1.2 Objectives

The main goal of this thesis is to explore 1D co-current spontaneous imbibition process and to develop a model using the IORCoreSim simulator, that can be applied to match and interpret the experimental data reported by Haugen et al., (2014, 2015). Throughout this study, the following tasks will be performed:

- Establish relative permeability and capillary pressure curves for a reference case by history matching the experimental data with the simulation tool.

- Once a match is successfully obtained, use the optimized saturation function curves to perform sensitivity analysis that studies the response of co-, counter- and total production by varying the following key parameters:
    - Mobility ratio by holding one viscosity fixed while changing the other
    - Equal scaling of the fluid viscosities at fixed mobility ratio
    - Capillary back pressure

2 THEORY

This chapter is intended to introduce the fundamental aspects of spontaneous imbibition and how the various concepts discussed explain the subject matter covered in this study. The idea is to build a rudimentary foundation that will present definitions to terminologies applied in this study and serve as a pivotal basis to adequately comprehend the complex systems and mechanism analyzed in this thesis work. For simplicity, all concepts are outlined by assuming a two-phase oil/water system within the fractured reservoir material. Also, imbibition is used in this work to mean the increase in water phase saturation whereas drainage means reduced water saturation.

2.1 Wettability

Wettability defines the tendency of one fluid to spread on or adhere to the surface of the reservoir rock in the presence of another immiscible fluid (Craig, 1971; Tarek, 2006). This tendency is referred to as the wetting characteristics of the fluid for the rock surface and the system can be water-wet, oil-wet, fractionally wet, or mixed-wet (Salathiel, 1973; Anderson, 1987). The present literature (Chilingar & Yen, 1983; Anderson, 1986; Cuiec, 1991; Rao, 1996 ; Donaldson & Waqi, 2008) reveals how that the prevailing wetting state of any reservoir system will influence the distribution of reservoir fluids, flow of fluid phases and directly impact the driving forces in the hydrocarbon system. Of key essence is its effect on the flow functions (relative permeabilities to oil and water) as well as its interplay with capillary pressure. Figure 2.1 presents an illustration of this inter-connection for a water-wet system. Knowledge of the wetting characteristics is important to properly understand the behaviour of any reservoir system and to interpret experimental and numerical results accurately.

In water-wet conditions, if the water saturation is reduced to its irreducible saturation (S_{wi}), water remains as a continuous phase in the small pores throughout the rock structure and the oil is reserved to larger pores with high enough saturation to exist as a continuous phase. A rock under such wetting state will spontaneously imbibe water (the wetting phase) to expel the oil (which is non-wetting) until a state of static equilibrium is reached between the capillary and surface energy forces (Donaldson & Waqi, 2008). As the water saturation increases, the oil phase experiences a snap-off effect, becoming discontinuous and existing as globules in the center of the larger pores. During oil recovery by spontaneous imbibition, the wetting state of a porous medium is important since the matrix must be able to draw in the water spontaneously. If the matrix is non-wetting, it will resist automatic water uptake.

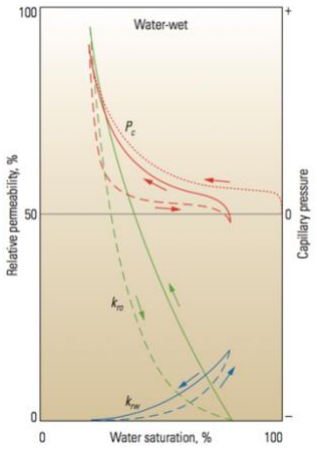

Figure 2.1: *Capillary pressure and relative permeability for water-wet conditions (Abdallah et al., 2007)*

2.2 Saturation functions

2.2.1 Capillary Pressure

When two immiscible fluids are in contact in the interstices of a porous medium, a pressure discontinuity exists across the curved interface separating the two fluids (Torsæter & Abtahi, 2003). This difference in pressure is the capillary pressure (Pc), which is pressure in the nonwetting phase (P_{NW}) minus the pressure in the wetting phase (P_W). Mathematically, capillary pressure for an oil-water system (water-wet) can be expressed as

$$P_c = P_{NW} - P_W = P_o - P_w \quad (2.2.1)$$

where *NW* phase is oil, *W* phase is water, P_o & P_w are the oil and water phase pressures across the interface respectively. Since oil is the non-wetting phase in a water-wet system, the capillary pressure value is positive.
An expression relating the capillary pressure with the radius of a capillary tube and the interfacial tension is defined as

$$P_c = \frac{2\sigma cos\theta}{r} \quad (2.2.2)$$

where σ - interfacial tension (*IFT*), θ - contact angle, r - pore channel radius.

Clearly, Equation 2.2.1 reveals the Pc as the excess pressure in the non-wetting fluid relative to the wetting fluid's pressure, whilst Equation 2.2.2 tells that higher Pc is required to invade the smaller pores in the reservoir. The capillary pressure that exists within a porous medium between two immiscible phases is a function of the interfacial tensions and the size distribution of the capillaries, which, in turn, control the curvature of the interface. In addition, the curvature is also a function of the saturation distribution of the fluids involved (Tarek, 2006).

This intricately makes the Pc a function of fluid saturation. Bear & Verruiit, (1987) described the empirical relationship between capillary pressure and saturation in the form:

$$P_{NW}^{avg} - P_W^{avg} = Pc = f(S) \quad (2.2.3)$$

where P_{NW}^{avg} - the average pressure of non-wetting phase, P_W^{avg} – the average pressure of wetting phase, P_c– capillary pressure, S – the wetting phase saturation.

Typical illustration of laboratory experiments to simulate the displacing forces in a reservoir to determine the magnitude of the capillary forces and thence, determine the fluid saturation distributions and connate water saturation, *Swc* (the maximum water saturation at which the water phase will remain immobile) is shown in Figure 2.2.

Originally, when oil invaded the reservoir rock, it was saturated with water. The pore size distribution will define the equilibrium saturation distribution after oil has migrated from source rock into the water filled pore space. This process is known as drainage, which occurs when the pressure in the oil phase exceeds the pressure in the water phase by a specific value. This value is called the reservoir threshold pressure *Pd* (see Figure 2.2), which is the pressure needed for oil to enter the largest pores in the distribution (Szymkiewicz, 2012). Furthermore, as the capillary pressure increases, the water saturation will approach irreducible water saturation *Swir*, in which no more water will be displaced. The *drainage process*

described (and shown in Figure 2.2) corresponds to the so-called primary drainage curve. This drainage process establishes the fluid saturations, which are found when the reservoir is discovered.

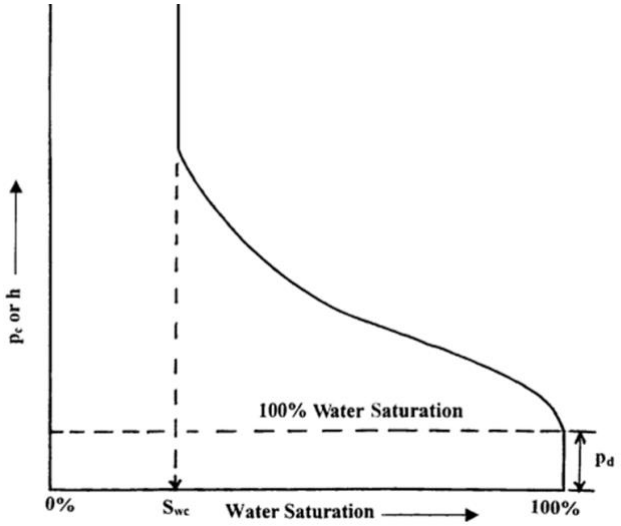

Figure 2.2: *Typical Capillary Pressure Curve (Tarek, 2006)*

A different principal flow process occurs when the oil saturated reservoir, upon discovery, is produced by displacing the oil with the wetting phase, water. *imbibition process* and the resulting curve is termed the *capillary pressure imbibition curve*. These two Pc curves follow different paths and is termed as c*apillary hysteresis*. McCardell, (1955) attributed this phenomenon to the variations in radius along the tortuous pore length of the reservoir medium and proposed a mechanism known as the ink-bottle effect.

Capillary forces are a decisive influence on oil recovery efficiency and could act against or in favor of the production depending on the formation framework. Displacement in fractured reservoir systems, like carbonates is only supported by positive capillary forces (Cuiec et al., 1994), which is substantial when the formation is preferentially water-wet. The strong capillary forces incited will encourage self-uptake of water through spontaneous imbibition to eject oil. This interplay of wetting state and capillary driving forces is noteworthy when considering oil displacement by SI. This spontaneous imbibition process will proceed until Pc = 0. In strongly water-wet systems, this happens until 1-Sor (where Sor represents the residual oil saturation). In mixed wet systems, Pc = 0 occurs as Sw < 1-Sor and so less oil is recovered by SI in such systems. Under such conditions, the extra oil can be produced by force imbibition, often achieved through injection of displacement fluid.

2.2.2 Relative Permeability

The tendency of a fluid to flow through a porous media is hugely dependent on the ability of the formation to transmit the fluid. This property is referred to as absolute permeability, represented as *k*. The simultaneous flow of oil and water causes each phase to interfere with the flow of the other and thus relative permeabilities are frequently used to represent the permeability of the phases by:

$$k_{rw} = \frac{k_w}{k} \leq 1 \ \text{, for water} \qquad (2.2.4)$$

$$k_{rw} = \frac{k_o}{k} \leq 1 \ \text{for oil} \qquad (2.2.5)$$

k_w and k_o are the effective permeabilities (i.e when the sample is 100% filled with the phase).

These flow parameters are unique functions of saturation. Thus, for a porous medium, the fluids are only mobile within a specific saturation range, which defined over the water phase is $S_{wir} \leq S_w \leq S_w^{max}$. The water relative permeability will vary from $k_{rw}(S_w = S_{wir}) = 0$ to a maximum value,

$k_{rw}(S_w = S_w^{max} = 1 - S_{or}) = k_{rw}^{max}$. Over the same range of saturation, the oil relative permeability will vary from a maximum value, $k_{ro}(S_w = S_{wir}\ or\ S_o = S_o^{max}) = k_{ro}^{max}$ to $k_{ro}(S_w = S_w^{max} = 1 - S_{or}\ or\ S_o = S_{or}) = 0$. This relationship is more conveniently represented by relative permeability curves, depicted in Figure 2.3.

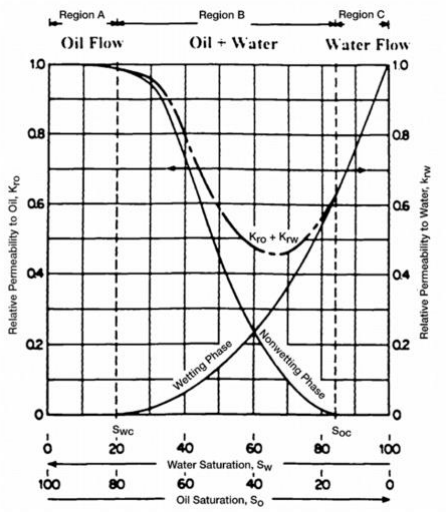

Figure 2.3: *Typical oil/water flow behaviour (Tarek, 2006).*

2.3 Spontaneous Imbibition

Imbibition is the process of absorbing a wetting phase into a porous rock. It is a key mechanism in water drive recovery from fractured reservoirs because it can hinder or advance water movement, affecting the recovery efficiency. The resident crude oil in the matrix has no inherent ability to drive itself out of the pores but rather is ejected by the accumulation of water in the pore spaces (Bourbiaux, 2009). This can the thought of as an elimination of crude oil out of the rock, by substitution with water; a phenomenon that would occur much more readily if the rock matrix has a preferentially higher affinity for the water than for oil (Anderson, 1987). The term spontaneous imbibition (SI), then, is when the absorption process occurs without any external force driving the water phase into the rock. Such uptake of wetting fluid into a porous medium is driven by capillary action and resisted by viscous forces. The relative magnitude of the interaction between these forces primarily dictates the imbibition rate (Morrow & Mason, 2001; Andersen et al., 2018a; Mason & Morrow, 2013). The SI process can be summarized in one illustration as presented in Figure 2.4.

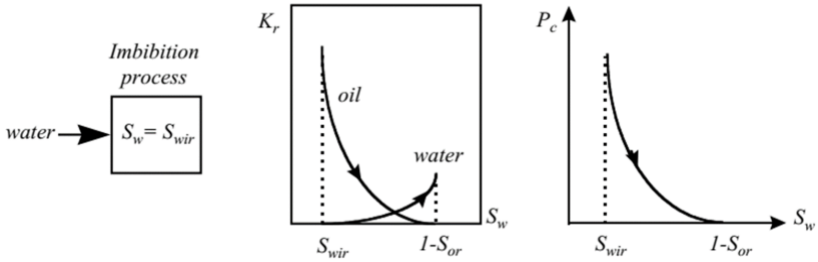

Figure 2.4: *Imbibition of water into a water-wet core filled with oil (Kleppe, 2014)*

2.4 Boundary Conditions

Standnes (2004) defined SI as the process where fluids are sucked into a porous medium by the action of capillary forces. During such fluid replacement process the relative direction defining the movement of the two fluid phases defines the ensuing mechanism.

These mechanisms are generally categorized into two main forms: Co-Current Spontaneous Imbibition (COCSI) and Counter-Current Spontaneous Imbibition (COUCSI). In COCSI, both Wetting (W) and Non-Wetting (NW) phases flow in the same direction, whereas flow for both phases is in the opposite direction during COUCSI (Li et al., 2003; Andersen et al., 2018a). In experimental investigations of SI, the distribution of fluid around the available permeable portions of the porous sample stipulates the resulting spontaneous mechanism. The exposure of different portions of the porous medium is usually referred to as the boundary condition (BC) and is a vital aspect that needs proper capturing during mathematical or numerical considerations of any SI experiment.

In laboratory SI experiments, different standard boundary conditions are applicable. The typical BCs implemented are: All Faces Open (AFO) (Mason et al., 2009; Fernø et al., 2014), One End Open (OEO) (Akin et al., 1998; Li et al., 2003), Two Ends Closed (TEC) (Fischer et al., 2006), Two Ends Open (TEO) (Bourbiaux & Kalaydjian, 1990; Yoldiz et al., 2006; Mason et al., 2010) and a special form of the TEO boundary condition (see Figure 2.5), Two Ends Open – Free Spontaneous Imbibition (TEOFSI), introduced by (Haugen et al., 2014).

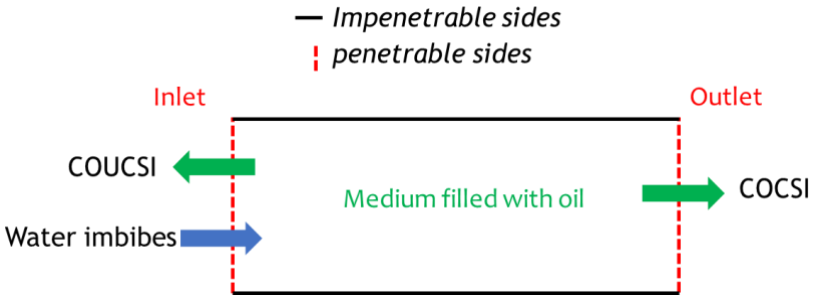

***Figure 2.5**: Illustration of the TEOFSI system introduced by (modified by Haugen et al., 2014).*

In this thesis work, only the standard Two-End-Open-Free Spontaneous Imbibition (TEOFSI) boundary condition is considered, as in relation to the experimental data under study. In the TEOFSI boundary condition, all sides of the porous medium are impenetrable to fluids, except two opposite end sides, where one end face of the core is exposed to the W phase and the other to the NW phase. The wetting phase (which is the imbibimg fluid) can only enter the core through the end face exposed to it (usually termed the inlet) whereas the non-wetting phase (which is pre-saturated into the core) can be produced at the inlet phase or at the opposite end face exposed to it (usually termed the outlet). Production of the NW phase at the inlet, then, becomes COUCSI and the outlet ejection occurs through COCSI. Foley et al., (2017) revealed that NW phase can only be produced co-currently, when its phase pressure exceeds the capillary back pressure (CBP). However, as pointed out by Haugen et al., (2014), during TEOFSI, several factors exercise control on when, or if, counter-current production stops (Andersen et al., 2018a). The CBP has been defined as the resistance for oil to be produced as droplets into the water phase at the inlet side (Andersen et al., 2017).

Fluid flow by TEOFSI progresses in 1D, which is less complex and easy to model mathematically, using established differential equations.

2.5 Mathematical Model

When water displaces oil spontaneously under the influence of capillary forces, a diffusion-advection equation model may be used to present an analytical solution for flow of immiscible fluids under both counter-current and co- current imbibition in strongly water-wet porous medium. Simplification is possible by considering a 1D horizontal formulation where gravity forces are negligible (relative to capillary forces) and fluid phases assumed to be incompressible.

The transport equations for oil (o) and water (w) in porous media are given by:

$$\varphi \frac{\partial S_l}{\partial t} = -\frac{\partial v_l}{\partial x} \qquad (2.5.1)$$

where φ - porosity, S_l- phase saturation and v_l- Darcy velocity of each phase.

Considering two-phase flow and the simplifications outlined, the generalized Darcy law is formulated as:

$$v_w = -\frac{kk_{rw}}{\mu_w}\left(\frac{\partial P_w}{\partial x}\right) \qquad (2.5.2)$$

$$v_o = -\frac{kk_{ro}}{\mu_o}\left(\frac{\partial P_o}{\partial x}\right) \qquad (2.5.3)$$

where $v_{w/o}$ – water/oil flux, k - absolute permeability, k_{rw}- relative permeability to water, k_{ro}- relative permeability to oil, $\mu_{w/o}$- viscosity for water/oil, $P_{w/o}$- water/oil phase pressure.

The saturation parameters for water and oil are constrained by volume conservation:

$$S_w + S_o = 1 \qquad (2.5.4)$$

Whereas the assumption of phase pressure equilibrium constrains the pressure parameters through the expression for capillary pressure:

$$P_c(S_w) = P_o - P_w \qquad (2.5.5)$$

Then, the total Darcy velocity v_T can be written in the following form:

$$v_T = v_w + v_o = -k\lambda_o \frac{\partial P_c}{\partial x} - k\lambda_T \frac{\partial P_w}{\partial x} \qquad (2.5.6)$$

where the mobilities (λ_w), (λ_o) and (λ_T) are defined as: $\lambda_w = \frac{k_{rw}}{\mu_w}$; $\lambda_o = \frac{k_{ro}}{\mu_o}$; $\lambda_T = \lambda_w + \lambda_o$.

For co-current flow, equation 2.5.1 through 2.5.3 can be transformed into a standard equation as presented by Andersen et al., (2017):

- P_w is eliminated with equation 2.5.5 since $P_w = P_o - P_c(S_w)$
- The S_o is replaced by 1-S_w, using the saturation constraint in equation 2.5.4
- The total velocity in 2.5.6 is introduced to eliminate the oil pressure P_o

Applying this procedure, the water transport equation can be written as a standard expression below (Chen et al., 2006):

$$\varphi \frac{\partial S_w}{\partial t} + \frac{\partial}{\partial x}\left(v_T f_w + k\lambda_o f_w \frac{\partial P_c(S_w)}{\partial x}\right) = 0 \qquad (2.5.7)$$

where $f_w = \frac{\lambda_o}{\lambda_w + \lambda_o}$ is the water fractional-flow function.

A pressure equation given below, must be solved together with equation 2.5.7 to obtain a solution to the system

$$\frac{\partial}{\partial x}\left(-k\lambda_o\frac{\partial P_c}{\partial x}-k\lambda_T\frac{\partial P_w}{\partial x}\right)=0 \qquad (2.5.8)$$

It is worthy of note that in co-current imbibition, the flow of oil and water in the same direction will imply that the pressure gradients of the two phases are oriented in the same direction. As a result, the displacement of the fluid with higher Darcy velocity will contribute positively to the flow of the other fluid. This interplay is commonly referred to as viscous coupling or Yuster effect (Babchin et al., 1998) and has a positive effect on co-current flow.

For counter-current imbibition, the fluids move in opposite direction of each other. This will generate a negative viscous drag on the interface between the two fluids and give a lower total velocity of the displacement process (Rose, 1988). Consequently, viscous coupling has a negative effect on counter-current flow in terms of fluid mobility.

The equations 2.5.7 and 2.5.8 are solved by specifying boundary and initial conditions for water and pressure distribution (see Figure 3.3). It is the proper definition of the boundary conditions that controls the mathematical derivation and conforms it to a TEOFSI system. The implemented conditions are presented later in this report under subsection 3.6.

2.6 The Buckley- Leverett Flow Theory

Buckley & Leverett , (1942) investigated the mechanism of fluid displacement and developed the Buckley-Leverett (BL) theory , which estimates the rate at which an injected water bank moves through a porous medium. The BL flow theory is based on the law of mass conservation during forced displacement process by the development of a fractional flow equation (Leverett, 1941) for oil and water.The fraction of water present in the advancing front during the displacement process is given by:

$$f_w=\frac{q_w}{q_w+q_o} \qquad (2.6.1)$$

Where f_w = fraction of water in the flowing stream; $q_{w,o}$= flow rate of the individual fluid phases

When the flow rate expression $q_w=v_l*A$ (see Equation 2.5.2) is implemented with the assumption of linear and horizontal flow through a core of cross-sectional area 'A', where gravity and capillary forces are neglected, Equation 2.6.1 can be written in the form (Tarek, 2006):

$$f_w=\frac{1}{1+\frac{k_{ro}\mu_w}{k_{rw}\mu_o}} \qquad (2.6.2)$$

The dependency of k_{rl} on saturation makes f_w a sole function of saturation when the fluid viscosities are constant. The f_w function is typified by an S-shaped curve and the saturation front that is formed can be determined by the tangent line of the fractional flow curve that extends to the initial water saturation.

Since S_w is a function of both time and position, classical mathematical computations performed on Equation 2.5.7 when the capillary diffusion term is set equal to zero and the inclusion of a shock front can allow for the construction of the water saturation profile (S_w versus distance along the core). The fractional flow curve and a typical saturation profile are depicted in Figure 2.6.

The effect of water and oil viscosities on f_w is clearly indicated by examining Equation 2.6.2. Regardless of the system's wettability, a higher μ_o results in an upward shift (increase) in the fractional flow curve whereas higher μ_w results in an overall reduction in f_w (downward shift of the curve) (Tarek, 2006).

The front saturation, therefore, is controlled by the Mobility ratio of the displacement process (this is presented in section 2.6).

In relation to the nomenclature used in Figure 2.6, S_{wf} is the front saturation, S_{wc} is the connate water saturation, S_{wbc} is the average water saturation at breakthrough. The saturation profile (Figure 2.6b) is depicted at a fixed time and it shows the maximum water saturation ($S_w = 1-S_{or}$) to have moved a distance X_1 whiles the front saturation, S_{wf} is located at position X_2 measured from the inlet side.

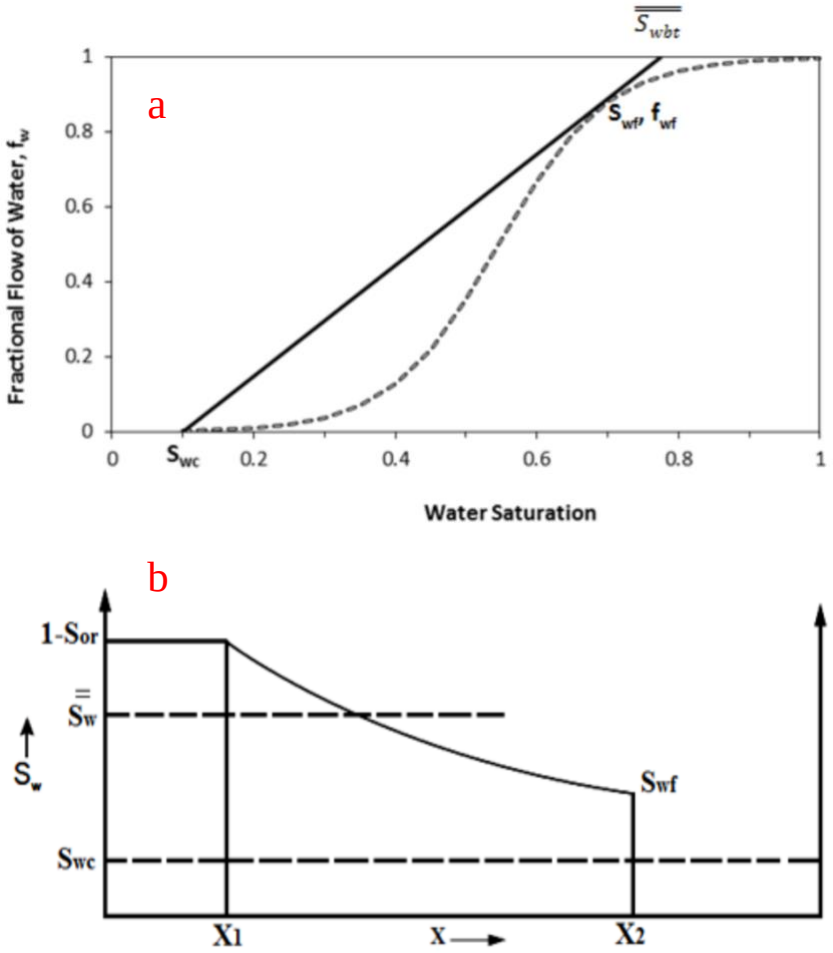

Figure 2.6: *Illustration of the BL-theory showing a fractional flow curve (a) and a typical profile of water saturation distribution as a function of distance before breakthrough (b) (Tarek, 2006).*

The imbibition of water into a core during TEOFSI has similarities to BL flow and the imbibition process can be assumed to progress according to a distorted Buckley-Leverett (BL) profile. This assumption is has been approved by some authors (Morrow & Mason, 2001; Andersen et al., 2018a; Andersen et al., 2018b) and was implemented in this thesis to interpret experimental data and to derive saturation functions used in the history match process.

2.7 Mobility ratio

The mobility of any fluid is the ratio of the effective permeability of the fluid to its viscosity ($\lambda_l = \frac{k_{rl}}{\mu_l}$). During the displacement of oil by water, the ratio of water mobility to oil mobility is defined as the Mobility ratio, M and given mathematically as (Muskat, 1946):

$$M = \frac{\lambda_w}{\lambda_o} = \frac{k_{rw}}{k_{rw}} \frac{\mu_o}{\mu_w} \qquad (2.7.1)$$

Muskat, (1946) points out that k_{ro} must be evaluated at initial water saturation because the displaced oil is moving ahead of the water front in the noninvaded zone, whereas k_{rw} will takes forms primarily dependent on the average water saturation in the invaded zone (which increases after water breakthrough). Relating Equations 2.7.1 and 2.6.2 expresses the influence of M (which is a saturation function) on the fractional flow function and the saturation profile.

In this study, by looking on the Corey-like correlation (see section 3.4) used to express the relative permeability function, M is computed by applying the maximum k_r values, k_{rw}^{max} and k_{ro}^{max} and M takes the form $M = \frac{k_{rw}^{max}}{k_{ro}^{max}} \frac{\mu_o}{\mu_w}$. By such definition of the mobility ratio, M can be altered simply by changing the viscosity ratio, $\frac{\mu_o}{\mu_w}$.

3 EXPERIMENTAL DETAILS AND NUMERICAL INVESTIGATION

This chapter presents the laboratory work considered as a basis for this thesis (physical model) and further reveals the concepts applied in the numerical study performed. Herein, the simulation tool used is presented together with the input data and grid information as well as the mathematical correlations used to match experimental data.

3.1 Experimental details

The simulation studies performed in this work is based on laboratory work performed by Haugen, et al., (2014, 2015). The experiments were performed using outcrop cylindrical chalk core plugs obtained from Ålborg, Denmark. The chalk composition was mainly calcite with permeability ranging 3 - 6 mD. During preparation of the cores it was ensured that only the end faces were open and penetrable to fluids. This ensures closure of all radial boundaries and the system can be considered as 1D.

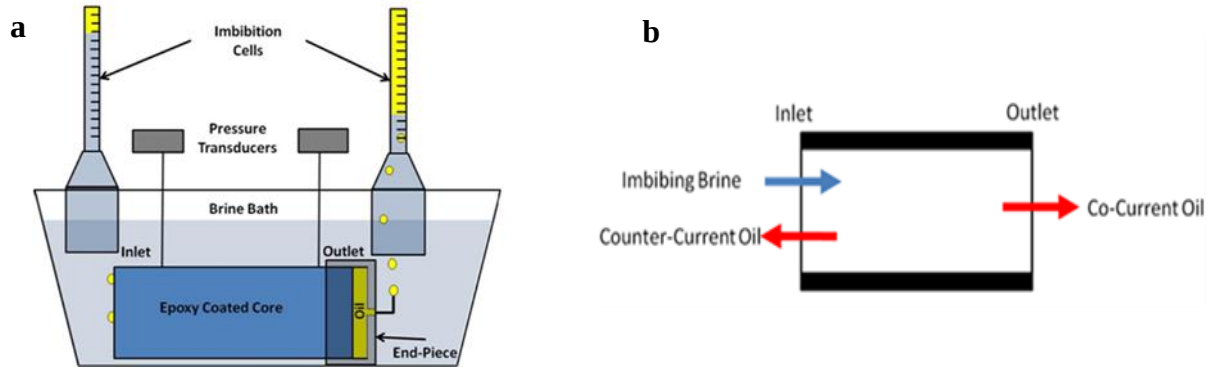

Figure 3.1: *(a) Schematic diagram of the experimental setup. (b) Boundary conditions and direction of flow during the experiment (Haugen, et al., (2014)*

Synthetic brine was used as the wetting phase and refined oil devoid of surface active components was used as the non-wetting phase. The boundary condition applied (Figure 3.1b) was the TEOFSI and Figure 3.1a shows how the inlet end of the core was kept in contact with the imbibing brine and the outlet end in contact with oil by means of an oil-filled void end-piece. Properties of the core material and fluid properties are presented in Table 3.1. The brine viscosity is fixed at 1.09cP while the oil viscosity is varied from 1.47cP to 137cP.

Table 3.1*: Core Material and Fluid Properties*

Core	Length (cm)	Diameter (cm)	Porosity (fraction)	Brine		Mineral Oil	
				ρ (g/ml)	*μ (cP)*	*ρ (g/ml)*	*μ (cP)*
CHP2	16.6	3.79	0.460	1.05	1.09	0.74	1.47
CHP11	3.1	3.81	0.466	1.05	1.09	0.87	137
CHP25	5.75	3.70	0.458	1.05	1.09	0.84	83.3

The core was initially 100% saturated with the oil and fully submergerd horizontally in the brine, to initiate spontaneous imbibition at the inlet end. Under such experimental set-up, co-current SI behavoiur is

favoured, with minor counter-current production. They termed the imbibition behaviour with this set-up as Two End Open Free Spontaneous Imbibition (TEOFSI).

The oil produced from each end was monitored using calibrated imbibition cells and presented as volume produced versus time. At the onset of imbibition, oil was produced from both end faces, counter-currently at the inlet face and co-currently at the outlet face. Oil production at the inlet phase ceases after a short period of time and the imbibition process is therafter, purely COCSI. The recorded recovery and fractional oil production during the SI are presented later in chapter 4.

3.2 IORCoreSim

The simulations studies conducted were run using IORCoreSim (Version 1.277), a development of BugSim. It is a combined EOR and SCAL simulator developed at the IOR Centre of Norway. The program, as outlined by Lohne (2017) is a three dimensional, rectangular or radial grid model that handles multi-component flow with up to three phases (water, oil and gas).

Previously, some authors (Andersen et al., 2017; Andersen et al., 2018a; Andersen et al., 2018b) have performed simulation studies using this simulator. In this thesis, the water and oil phases were considered as immiscible and incompressible, this was applied to model the system during spontaneous imbibition of brine. The simulator solves the four variables (oil and water saturations and pressure) within each matrix domain. In the program, the main flow fields are computed from a finite-difference discretization, using a sequential solution method (Watts, 1986) for both pressure and saturations (Andersen et al., 2018b).

In accordance to standard procedure, at any timestep, the pressure field is calculated first, using linear pressure equation by keeping the saturation-dependent variables fixed at the values form the previous timestep. Next, the phase velocities are updated by solving an additional saturation equation formulated in terms of the water fractional-flow function. The fractional flow equation is solved implicitly with respect to relative permeability and capillary pressure whilst keeping the oil pressure and total flowrate from the pressure solution constant.

The required input for all the simulations run are summarized below:

- Core dimensions and properties (diameter, length, porosity, permeability)
- Fluid properties (viscosity, density, oil/water interfacial tension)
- Saturation functions (relative permeability, capillary pressure)
- Boundary conditions (pressure, contacting fluid at the end faces)

Majority of the required input were measured and presented in the experimental work as shown in Table 3.1. The input saturation functions were obtained through correlations and are presented in sections 3.3 and 3.4.

3.3 Capillary Pressure Correlation

For numerical investigations of the displacement processes, it is convenient to express the Pc as an analytical function defined in terms of its controlling parameters. Leverett (1929) used a parallel bundle of tubes of equal radius, r, to define a microscopic radius in terms of permeability, k, and porosity, φ.

$$r = \sqrt{\frac{8k}{\varphi}} \qquad (3.3.1)$$

He further derived a relation between the Pc and a dimensionless parameter known as the Leverett J-function (Leverett, 1941) which could be employed to upscale laboratory data to classify the capillary state of a whole reservoir. He defined the J-function as:

$$J(S_w) = \frac{P_c}{\sigma}\sqrt{\frac{k}{\varphi}} \qquad (3.3.2)$$

where $J(S_w)$ – scaled Leverett function, P_c – capillary pressure, (bar), σ – interfacial tension, (mN/m), k – permeability, (mD), φ – fractional porosity.

The capillary pressure curve, in dimensionless form, is included as an input for the numerical model using the IORCoreSim, as tabulated values for corresponding water saturations. Consequently, it was decided to use the correlation proposed by Andersen et al., (2017) which is generally given as

$$J(S) = \frac{a_1}{(1+k_1 S)^{n_1}} - \frac{a_2}{\left(1+k_2(1-S)\right)^{n_2}} + a_3 \qquad (3.3.3)$$

Where S is scaled water saturation defined by :

$$S = \frac{S_w - S_w^{min}}{S_w^{max} - S_w^{min}} \qquad (3.3.4)$$

where S_w^{min} and S_w^{max} are the initial saturation and maximum saturations (taken as 1-S_{or}) respectively obtained during the imbibition process such that the entire correlation is defined over the range $0 \leq S \leq 1$.

Such that $J(S=0) = J^{max}$, and $J(S=1) = J^{min}$. Here, J^{max} is the maximum dimensionless pressure which is obtained at the lowest considered water saturation and J^{min} is the minimum dimensionless pressure which is obtained at the highest considered water saturation.

If the curve parameters [$a_1, a_2, k_1, k_2, n_1, n_2$] > 0 the correlation is monotonously decreasing for any value of a_3 and thus the parameters can be chosen to fit experimental data for all wetting conditions with ease and high accuracy. Several other correlations exist in the literature (Brooks & Corey, 1964; Bentsen & Anli, 1977; O'Carrol et al., 2005; Skjæveland et al., 2000; Lomeland et al., 2008; Neshat & Pope, 2017), but this particular correlation proposed by Andersen et al., (2017) was selected especially due to its flexibility and accuracy for strongly wet media.

For strongly water-wet system, as considered in this thesis work, Equation 3.3.3 is simplified by setting $a_2 = 0$ and defining the constant term a_3 in such a manner that the relevant threshold value is obtained.

$$a_1 = \frac{(J^{max} - J^{mid})(1+k_1)^{n_1}}{(1+k_1)^{n_1} - 1}, \; a_2 = 0, \; a_3 = J^{max} - \frac{(J^{max} - J^{mid})(1+k_1)^{n_1}}{(1+k_1)^{n_1} - 1} \qquad (3.3.5)$$

Substitution into Equation 3.3.3 yields the final relation applied in this study;

$$J(S) = \left\{\frac{(J^{max} - J^{mid})(1+k_1)^{n_1}}{(1+k_1)^{n_1} - 1}\right\}\frac{1}{(1+k_1 S)^{n_1}} + \left\{J^{max} - \frac{(J^{max} - J^{mid})(1+k_1)^{n_1}}{(1+k_1)^{n_1} - 1}\right\} \qquad (3.3.6)$$

By assuming the capillary pressure to scale according to the Leverett expression, the obtained values are used as direct input for the simulation run. The scaled J-function is assumed to be independent of inherent fluid and rock properties.

3.4 Relative Permeability Correlation

The relative permeability functions are implemented as tabulated values when applying the IORCoreSim tool. Several correlations are available in the literature for prediction of two-phase water/oil relative permeability. The most common correlations are summarized in a study published by (Siddiqui et al., 1988; Baker, 1988). The correlation used in this study was adapted as a linear form of the Corey correlation (Corey, 1954) which was developed as a power law in the water saturation.

The Corey relative permeability equations for water and oil phases are:

$$k_{rw} = (S^*)^{n_w} \qquad (3.4.1)$$

$$k_{rw} = (1 - S^*)^{n_o} \qquad (3.4.2)$$

where the exponents are termed as core exponents and the normalized saturation given as;

$$S^* = \left(\frac{S_w - S_{wir}}{1 - S_{wir}}\right) \qquad (3.4.3)$$

The Corey-like functions as used by (Andersen et al., 2018a) was applied in this thesis to model the relative permeabilities for water and oil with slight variation of the mobile saturation range for the two phases. The functions are given as;

$$k_{rw} = k_{rw}^{max} * S_w^{E_w} \quad \text{and} \quad k_{ro} = k_{ro}^{max} * S_o^{E_o} \qquad (3.4.4)$$

Where the exponents were computed to vary linearly according to

$$E_w = E_{w,0}(1 - S_w) + E_{w,1}S_w \quad \text{and} \quad E_o = E_{o,0}S_o + E_{o,1}(1 - S_o) \qquad (3.4.5)$$

The normalized saturations in Equations 3.4.4 and 3.4.5 are given as;

$$S_w = max\left(0, \frac{s_w - s_{wr}}{1 - s_{or} - s_{wr}}\right) \quad \text{and} \quad S_o = 1 - S_w \qquad (3.4.6)$$

By such analytical notations, both phases have mobilities defined over the same saturation interval.

3.5 Numerical Grid

The numerical model was built using the Cartesian coordinate grid. A 1D Cartesian model was constructed and subdivided into 100 grid cells, where Nx:Ny:Nz equals 100:1:1 in the cartesian x, y and z-directions respectively.

The experimental set-up is a Two End Open Free Spontaneous Imbibition (TEOFSI) system and thus fluid flow into and out of the core is along the same horizontal axis (1D flow). It is somewhat justified to simulate in Cartesian 1D so as to capture the details in the fluid distribution that will give better detail of the saturation profile along the core during imbibition.

The experimental core geometry is cylindrical and thus the cross-sectional area transforms into the height and breadth of the rectangular grid model with the length corresponding exactly to the core length. This is depicted in Figure 3.2.

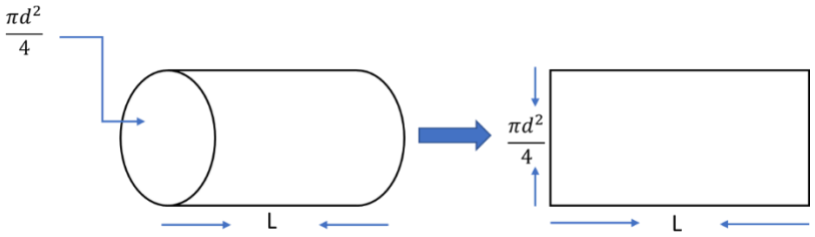

Figure 3.2: *Illustration of transformation from a cylindrical to a coordinate layout*

3.6 Initial and Boundary Conditions

The derivations that follow are presented with reference to Figure 3.3 which represents the geometry of the experimental set-up considered in this thesis. In the Figure, * and ** represent Equations 3.6.2 and 3.6.4 respectively.

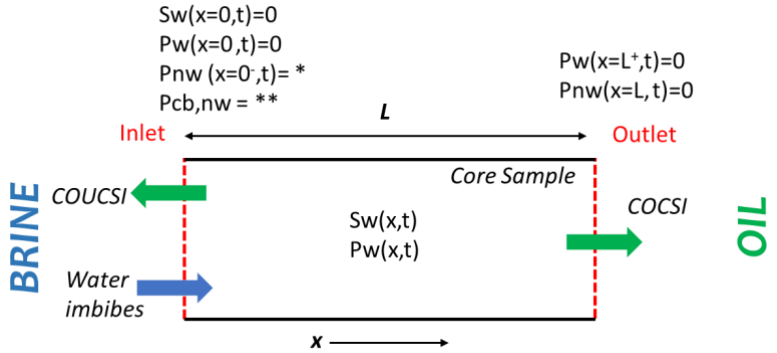

Figure 3.3: *Geometry of the TEOFSI system representing a water-wet core of length L. modified from Andersen et al., (2018)*

The laboratory data considered in this thesis used porous media fully saturated initially with oil as the non-wetting (*NW*) phase. The initial state of the system (see Figure 3.4) then follows as presented by Andersen et al., (2018a):

$$S_w(x, t = 0) = 0 \;; \quad (0 < x < L) \qquad (3.6.1)$$

The conventional TEOFSI boundary condition is applied to define the system, as in accordance to the laboratory setup. The relevant boundary conditions defined below are implemented by considering x = 0 as the water exposed end face (inlet) and x = L as the oil exposed end face (outlet). 0^-

BC at inlet:
$$P_{nw}(x = 0^-, t) = min\left(P_{nw}(x = 0^+, t), P_{cb,nw}\right) \qquad (3.6.2)^*$$

$$P_w(x = 0, t) = 0, \qquad (3.6.3)$$

$$P_{cb,nw} = \sigma\sqrt{\frac{\varphi}{K}} * J_{b,nw} \qquad (3.6.4)^{**}$$

The inlet BC modelled after this fashion will allow for counter-current production of the NW phase at the inlet if the internal NW phase pressure, P_{nw}, exceeds the *NW* phase capillary back pressure, $P_{cb,nw}$. However, if it is lower, the system switches to a no flow condition for the NW across the inlet.

BC at outlet:
$$P_{nw}(x = L, t) = 0, \qquad P_w(x = L^+, t) = 0 \qquad (3.6.5)$$

Here, the outlet, which is in continuous contact with the NW phase is defined as having zero external pressure in both phases. Across the outlet, the wetting (*W*) phase flux is set equal to zero by defining the *W* phase pressure discontinuous across the end phase until its pressure exceeds the external NW phase

pressure. As pointed out by Andersen et al., (2018a), this restrictive flow of the W at the outlet face does not occur in a strictly homogeneous, purely-capillary-driven TEOFSI system. Rather, $P_w(x = L^-)$ is computed from $P_{nw}(x = L)$ and the capillary pressure.

3.7 History Matching

It was adopted a method characterized by repeated and varied attempts which were continued until reaching satisfactory results to history match the experimental data. Here, the data to be matched was run with the same defined input and changes rendered according to observed deviation of the simulated result from the experimental data until an acceptable match is obtained. Variations in the input parameters (see subsection 3.2) are done based on the knowledge of how the different parts of the simulated curve-fit are affected by any specific input.

The imbibition of water into the core during TEO SI can be assumed to progress according to a distorted Buckley-Leverett (BL) profile, where the mobility ratio of the two phases controls the saturation front and a smearing that occurs due to capillary pressure gradient within the core. Generally, the saturation functions outside the BL shock front defines the characteristics of the displacement process. Specifically, the saturation interval between the front saturation, S_f, and the maximum saturation, 1-S_{or}, and the interval between S_f and the saturation value at initial water saturation, S_{wi}.
The experiments to be modelled were conducted with varying NW phase viscosities, where CHP11 contained the highest oil viscosity and CHP2 the lowest. By the assumption of a BL saturation profile, SI in CHP11 will therefore have lower front saturations and would require the largest saturation interval to properly define the displacement process. This experiment was therefore considered as the base to determine the saturation functions between S_f and 1-S_{or}. In the case with low NW phase viscosity, the displacement process develops sharp fronts with high front saturations and the behaviour is mainly dependent on the end-point values of the saturation functions and not necessarily the intermediate saturations since these occur in a limited fraction of the system. The experiment in CHP2 is therefore used to determine the end-point W phase relative permeability and the threshold P_c.

Notably, in the system with high oil viscosity (water mobility high comparable to oil), the front advance of the system is controlled both by the level of the relative permeability and the capillary pressure. Variations in the imbibition rate will be dependent more on the saturation distribution as dictated by the total mobility and the capillary pressure curve. Therefore, the case with high NW phase viscosity is expected to be sensitive to larger parts of the P_c and k_r curves whereas the case with lower NW viscosity will be affected only by the last part of the k_{rw} and P_c curves. These principles were applied in tuning the input parameters.

The experimental results also had low variance is the S_{or} thus this parameter was kept constant in the history match process. A residual water saturation was also assumed to account for the logicality of some water accumulation before water can advance. The representative functions for P_c and k_r were made flexible enough to allow for variations in specific parts of the curve during each trial of the run. The correlations used allowed for specific tuning of the curves at specific saturation ranges (low, mid or high saturation values) to properly incorporated the known principles of the system's behaviour into the matching process. The extent of counter-current oil production is sensitive to the capillary back pressure, P_{cb} and increases with increasing NW phase viscosity; this is accounted for in the matching as well. The boundary P_{cb} is set to zero for the outlet boundary, to prevent production of water in the present simulations. A boundary P_{cb} was specified at the inlet boundary. The value, on dimensionless form, was

J_{ob} = 0.08 in all the simulations. The value was not varied because it had very little effect on the production, since it was lower that the threshold P_c. Since the considered experiments were conducted under similar conditions and the Portland chalk reported as dominantly homogeneous, the same relative permeability and dimensionless capillary pressure curves were used to model each experiment.

This assumption will imply that the effect of viscous coupling on the relative permeability through its influence on the flow regime is neglected in the simulation process to history match the experiments. The applied matching procedure has been successfully implemented in previous numerical studies (Andersen et al., 2017; Andersen et al., 2018a; Andersen et al., 2018b) to match saturation functions in low permeable chalk experiments.

4 RESULTS AND DISCUSSIONS

This section presents the results of the simulation study with an attempt given to analyze the observed trends during sensitivity analysis of the system. The discussion is conducted in relation to the established literature. In the presentations that follow (especially for the plots), inlet refers to the side of the core exposed to water whereas outlet refers to the side exposed to oil (see Figure 3.1b).

4.1 History matching

The relative permeability functions k_{rw} , k_{ro} and scaled capillary pressure J-function were deduced from manual history matching of all experimental data and resulted in a reasonably good match to experimental observations for all experiments (CHP2, CHP11 and CHP25). The final optimised relative permeability and J-function curves applied to model the experiments are depicted in Figure 4.1, with the equivalent parameters in relation to the applied correlations shown in Table 4.1. The generated numbers are available in Appendix A1.

The J-function was adapted to finite values in the lower saturation range where mainly the magnitude could be determined from matching. At $S_w = 1-S_{or}$ the input capillary pressure was set equal to zero to establish a threshold J-value of 0.09. Such an adaptation of the Pc curve at $1-S_{or}$ was implemented to capture the Pc behaviour at the inlet end during counter-current production, where the NW phase is forced as droplets through the pores filled with water. Under such phenomenon, there is often a finite capillary pressure necessary to force the NW phase out. Similar adaptation was implemented successfully by Andersen et al., (2018b).

Table 4.1: *Key input parameters used to generate P_c and k_r curves used in all simulations (all parameters are dimensionless).*

Relative Permeability Parameters		Capillary Pressure Parameters		End-Point Saturations	
k_{rw}^{max}	0.16	J max	0.8	S_{wi}	0
k_{ro}^{max}	1	J min	0.09	S_{wir}	0.04
$E_{w,0}$	5	n1	0.8	S_{or}	0.34
$E_{w,1}$	2.3	k1	3.3		
$E_{o,0}$	0.38	a1	5.0097		
$E_{o,1}$	1.3	a3	0.9097		

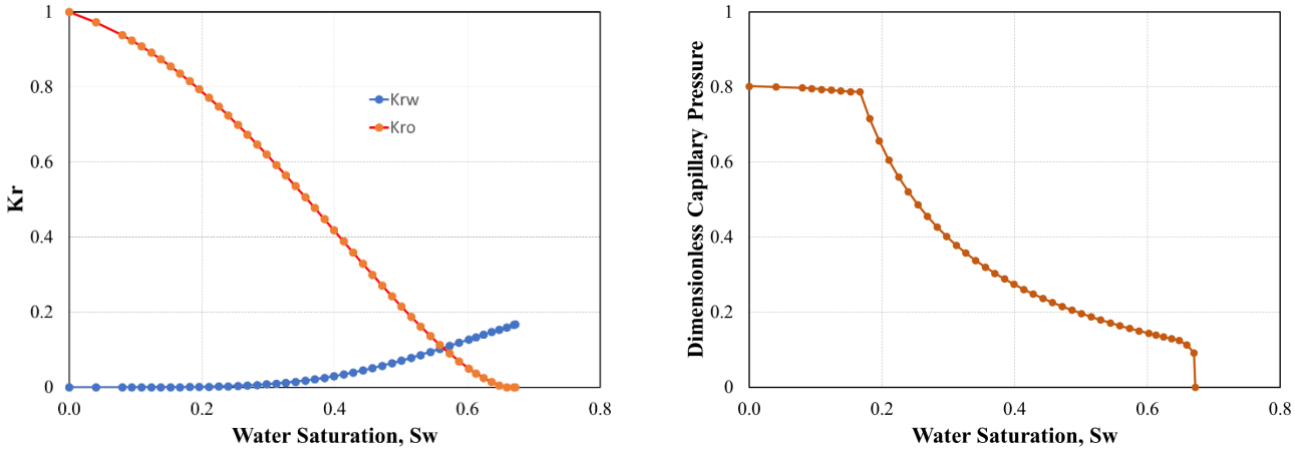

Figure 4.1: *Optimized relative permeabilities (left) and Dimensionless imbibition capillary pressure used in history matching of experiments.*

4.1.1 History Matching CHP 2

The experiment on CHP2 was conducted with the lowest NW phase viscosity (μ_o=*1.47*) and represented the case with the lowest viscosity ratio μ_o/μ_w equal to 1.35. The simulation was performed at ambient conditions with the specified TEOFSI boundary condition and the result is depicted in Figure 4.2.

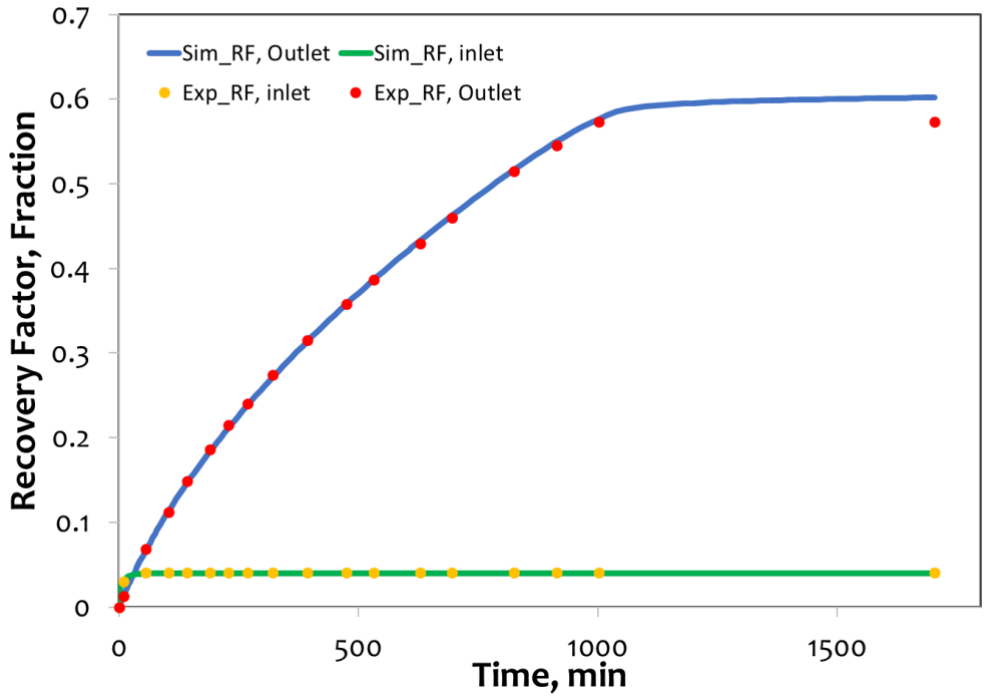

Figure 4.2: *History match of test CHP2 (μo=1.47cP) comparing experimental (markers) and simulated recovery factor versus time. The figure shows both counter current (inlet) and co-current recovery (outlet).*

By comparing, it is clearly seen how that the experimental recovery trend is well captured by the numerical model. The co-current production of oil at the initial stages is captured together with the observation of its abrupt no-flow, after which the oil is produced by pure co-current process. The predicted breakthrough (BT) time is slightly delayed (simulated 1120 min compared to measured 1000 min). Breakthrough here, refers to the arrival of water at the core outlet. In classical sense, the water does not flow through the outlet end and can be inferred to as the time when S_w takes a non-zero value in the last grid cell. Thereafter, S_w simply rises as more water accumulates and is captured in the recorded data as a change in production trend by a reduction in co-current production rate.

The model underestimates the total countercurrent RF by a value which represents a deviation of 0.1% whereas the co-current RF is overestimated by 2.9%.

4.1.2 History Matching CHP 11

The experiment on CHP11 was conducted with the highest NW phase viscosity (μ_o=*137*) and represented the case with the highest viscosity ratio μ_o/μ_w equal to 125.7. A comparison between the experimental data and the model is shown in Figure 4.3. In general, the simulation closely approximates the recovery output very well, especially in the early times (until 1000min) and towards the production plateau (2500 – 5900 min). The time duration between 1000 to 2500 min represent the section with a well-defined variance (up to a maximum underestimation of 0.03 in RF) between the match for the inlet production.

The overall co-current recovery is satisfactorily matched with a negative deviation of 0.03% whereas production at the inlet is underestimate by 3%. The match at early time is shown in Figure 4.4 to detail on the match-fit before 1200min. Here, it is observed how that the curve shape is well reproduced at the early stages. The breakthrough is not easily ascertained from the curves, but the simulated results depict an earlier breakthrough (~690min) as compared to the measured data (~860min).

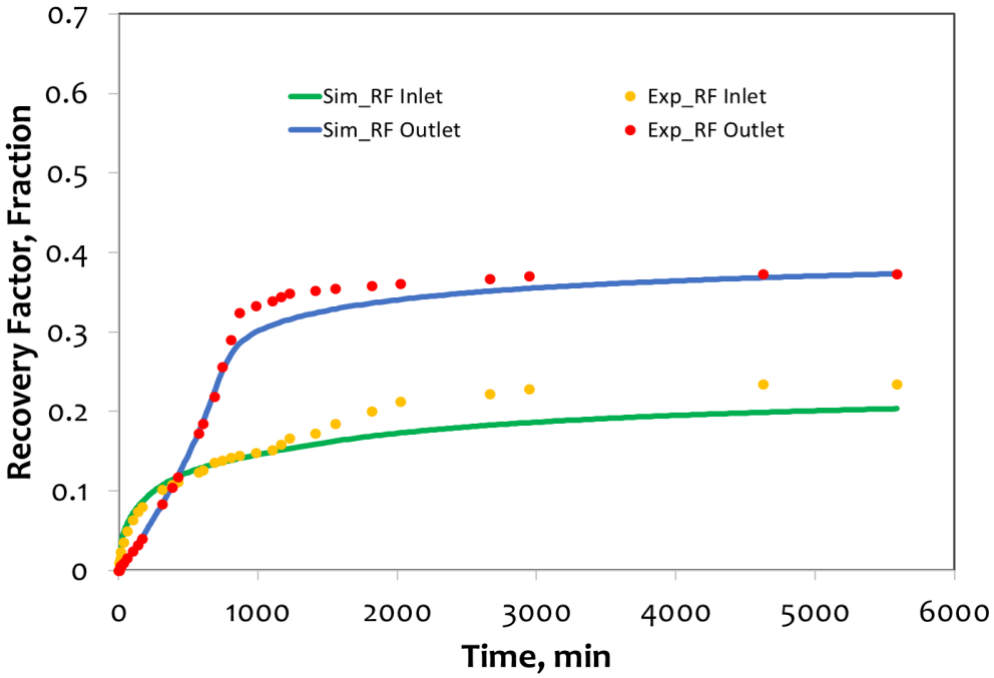

Figure 4.3: *History match of test CHP11 (μo=137cP) comparing experimental (markers) and simulated recovery factor versus time. The figure shows both counter current (inlet) and co-current (outlet) RF.*

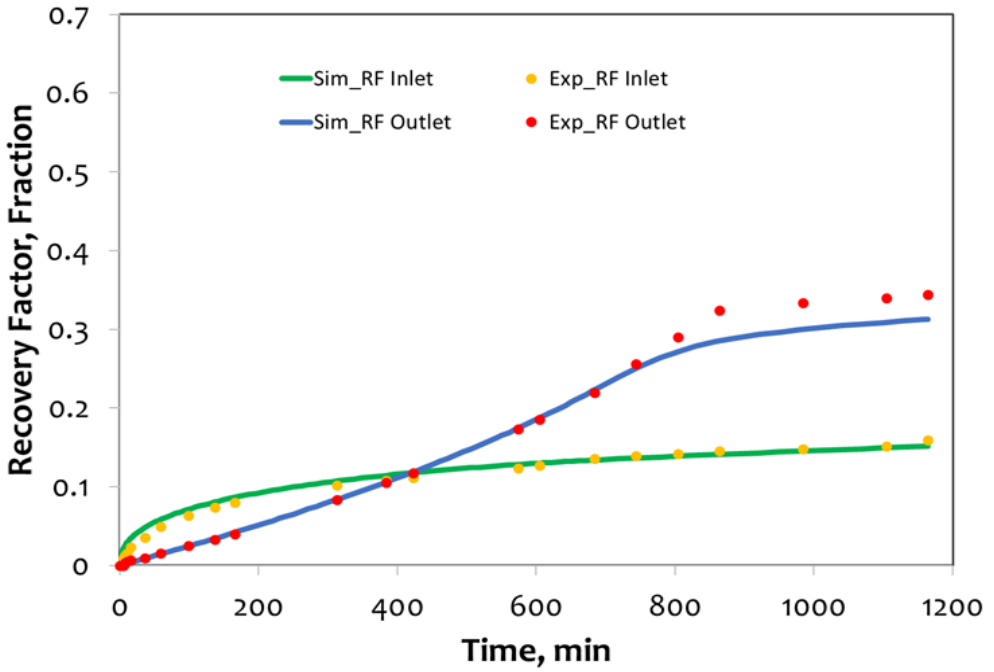

Figure 4.4: *History match of test CHP11 showing recovery factor versus time until 1200min..*

4.1.3 History Matching CHP 25

The experiment on CHP25 was conducted an NW phase viscosity intermediate to the two prior experiments (μ_o=*83.3*) and represented the case with an intermediate viscosity ratio μ_o/μ_w equal to 76.42. Figure 4.5 presents the comparison of the numerical results and the experimental data.

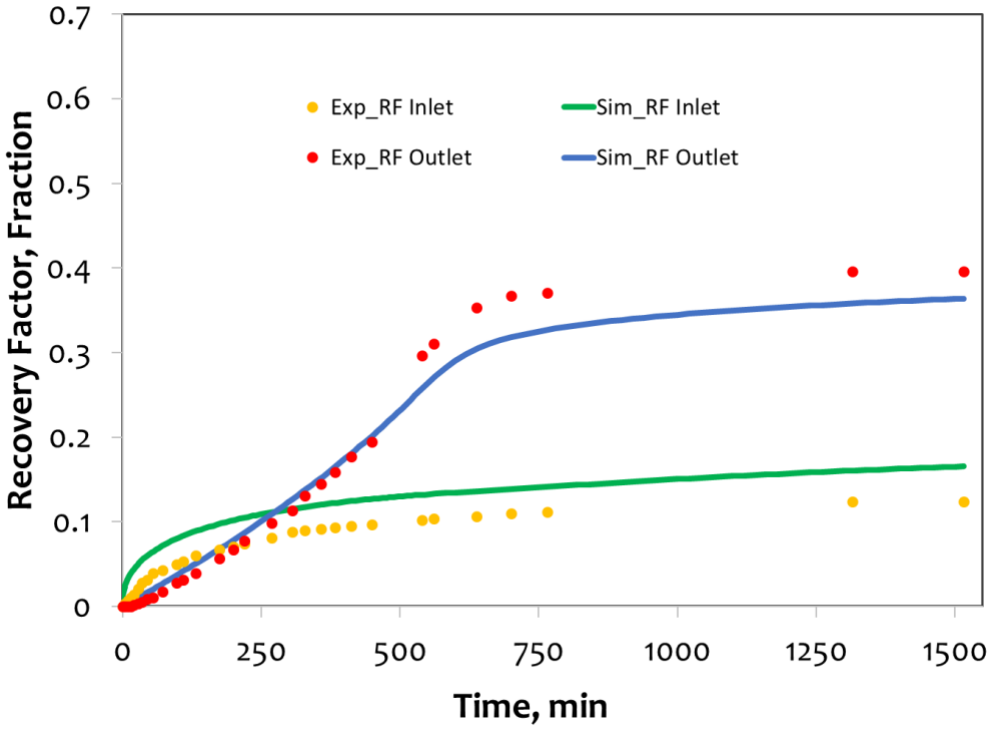

Figure 4.5: *History match of test CHP25 (μo=83.3cP) comparing experimental (markers) and simulated recovery factor versus time. The figure shows both counter current production (inlet) and co-current production (outlet)*

The model is seen to match the experimental data to an acceptable degree. The total co-current production is overestimated by 4.1% whereas the production at the inlet face is underestimated by 3.2%. The breakthrough time seems to be well approximated by the simulation (~530min as compared to the measured data~540min). The inlet production is nearly uniformly overestimated (ranging ~0.05 to ~0.02 difference in the RF). It is observed that the loss in outlet production depicted by the model is captured as an increase in the production at the inlet. Overall, the model overestimates the total recovery (inlet + outlet) by 1%.

The numerical model, therefore can be regarded as a good fit for the experimental data investigated and seeing as history matching is in itself subjective, it is possible that other matching parameters may exist that could also match the experimental results examined herein.

In principle, the cases with higher NW viscosity are sensitive to larger parts of the capillary pressure and relative permeability curves and thus the overall match can be further improved by further modifying these curves. However, this may require enormous efforts since the matching was done manually. The assumption that k_r is not influenced by viscous drag could be one issue to look upon as well. A comparison of the history match results are depicted in Figure 4.6.

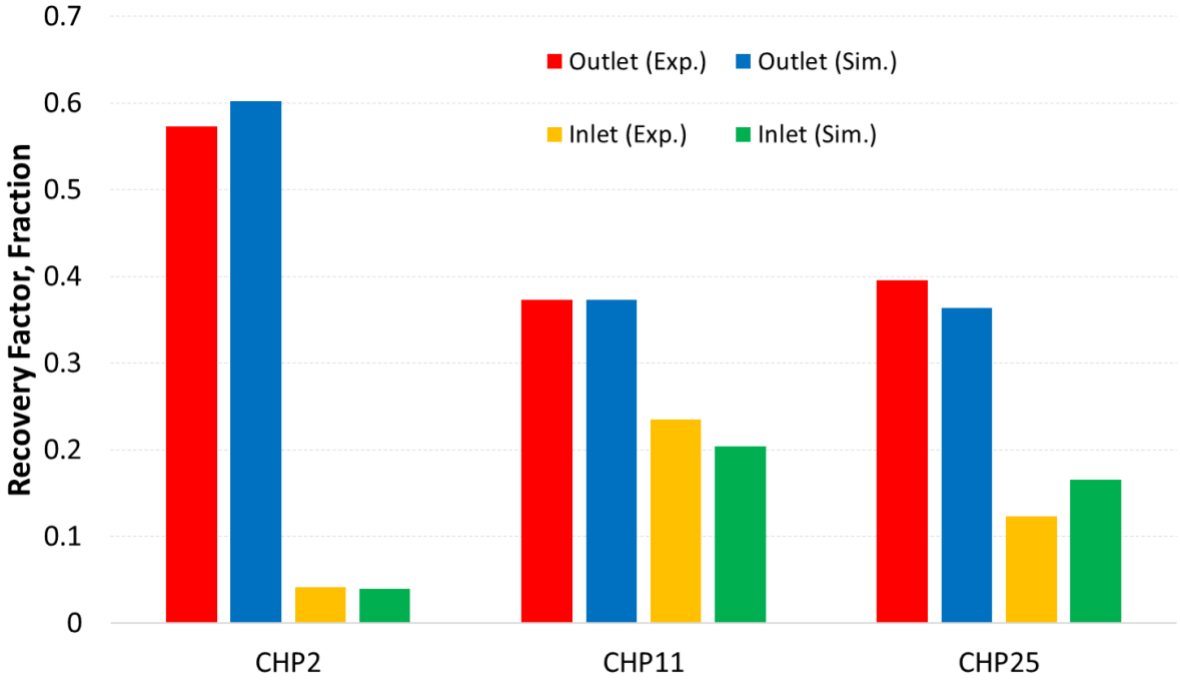

Figure 4.6: *Comparison of spontaneous oil production in experiments and simulations. The figures show co-current recovery (outlet) and counter-current recovery (inlet).*

4.2 Sensitivity analysis

A sensitivity analysis on the results was performed to better understand how the system works under different conditions. The established history match for the experiment conducted with CHP2 was used as the reference case for making the sensitivity analysis.

4.2.1 Varying Oil Viscosity at fixed water viscosity

The experiment conducted on CHP2 yields a Mobility Ratio, $M = \left(k_{rw}^{max}/\mu_w\right)/\left(k_{ro}^{max}/\mu_o\right) \approx 0.2$. The water and oil viscosities used were μ_w^{ref} *=1.09cP* and μ_o^{ref} *=1.47cP* respectively, with an established viscosity ratio μ_o/μ_w equal to 1.35. In Figure 4.7, model simulations conducted with varied oil viscosities (μ_o*=1, 32 and 1000 cP*) at fixed water viscosity are presented. This is recognized as an increase in the viscosity ratio $\frac{\mu_o}{\mu_w}$.

The recovery trends are different, with μ_o*=1cP* resulting in the longest breakthrough time (~1000min, Figure 4.7a) followed by the run with μ_o*=32cP* (~2500min, Figure 4.7b) and μ_o*=1000cP* produicng the earliest BT time (~12600min, Figure 4.7c). These approximate BT times are inferred from the point on the RF versus time curve where the co-current production rate decreases (Figure 4.7 b & c) or flattens (Figure 4.7a). For the same system, increasing only the oil viscosity will cause more oil to be trapped behind the imbibing front. This reduces the relative permeability to water behind the front, causing a slow imbibition rate and delaying the breakthrough time.

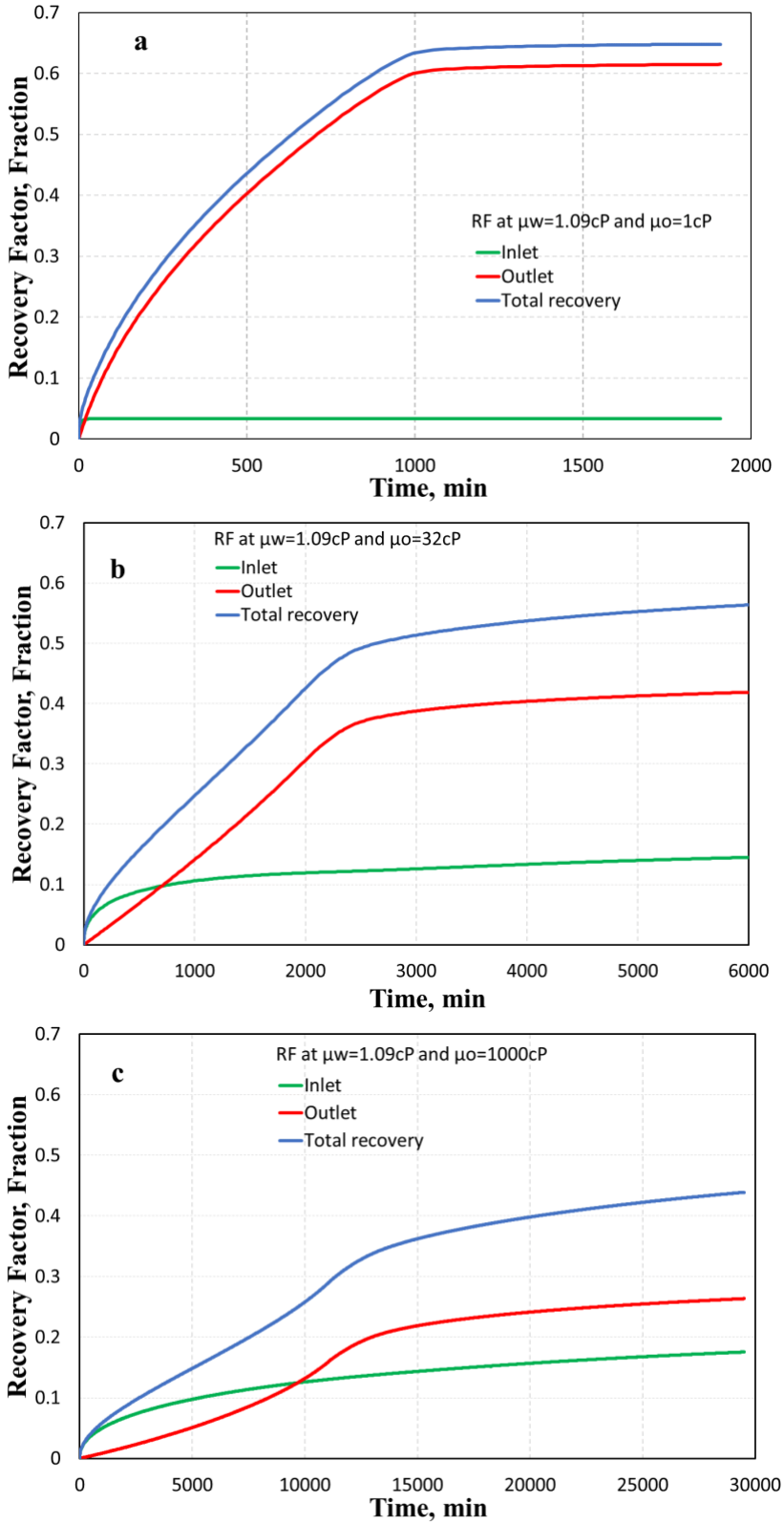

Figure 4.7: *Simulated RF versus time of CHP2 at fixed μ_w=1.09cP and varying μ_o=1cP (a), 32cP (b) and 1000cP (c). The figures show counter-current (inlet), co-current (outlet) and total RF.*

From Figure 4.7a-b, the co-current production plateau is decreasing with oil the increase in oil viscosity (0.61 > 0.41 > 0.26) whereas the counter-current production shows a reverse trend (0.03< 0.14 < 0.18). It is also observed that the counter-current imbibition time is relatively longer when the oil viscosity is increased. The total recovery factor decreases with increasing oil viscosity (0.65 > 0.56 > 0.43) and depicts that more oil is entrapped when oil viscosity is increased at a fixed water viscosity. Similar observation has been reported by Meng et al., (2015).

In Figure 4.7b, co-current recovery proceeds linearly until a time of nearly 2400min A similar uniform trend is observed in Figure 4.7c but terminates after approximately 5000min where the recovery suddenly increases with time till about 12600 where it declines towards a possible plateau. There appears to be a delay in the imbibition process that results in an S-shaped profile between times 5000min and 15000min. Delay in the onset of imbibition has been reported in published studies (Zhou et al., 2000; Morrow et al., 2001; Mason et al., 2013; Andersen et al., 2018b). The observed probable induction occuring with μ_o=*1000cP* (Figure 4.7c) is not seen in the other systems. It is likely that as water saturation builds up at the outlet, the oil mobility at the outlet is reduced and the whole system appears to have a high overal mobility.

A noticeable remark is the trend in recovery after the breakthrough time is reached. It appears that increasing the viscosity lowers the chance of reaching a production plateau and thus, though the water reaches breakthrough at an earlier time, production continues much longer afterwards. Haugen et al., (2014) made a similar observation and asserted that counter-current imbibition may progress for almost the entire imbibition period when the oil viscosity is increased relative to the water viscosity.

In Figure 4.8, the water saturation distribution along the core for the systems of increasing oil viscosity is presented. It is worthy of note that the front arrival at the outlet captured by the saturation profiles is captured at an earlier time that that observed in the plot of recovery factor versus time. The breakthrough time seen for Figure 4.7a is ~1000min but the actual arrival at the outlet occurs at ~700min (Figure 4.8a). The saturation profile reported in Figure 4.8 captures the time when the water saturation is non-zero in the outlet grid cell. This arrival time is however not immediately captured in Figure 4.7 since noticeable change in the co-current production rate is rather observed later, when water saturation builds up at the outlet to cause a substantial reduction in the mobility of oil at the outlet. Nonetheless, the possibility to approximate breakthrough time from recovery data is remarkable since this is impossible to observe in experimental proceedings conducted in a closed system.

The plots presented in Figure 4.8 reveals the behaviour of the system at times equal to half BT and twice the BT. It is observed that the system with μ_o=*1cP* (Figure 4.8a) initially progresses with a piston-like displacement front until a quarter of the core length is passed, where the water saturation at the front declines with time as more oil is bypassed. There is much smearing of the saturation profile and reduction in the water saturation at the front as oil viscosity is increased relative to water viscosity.

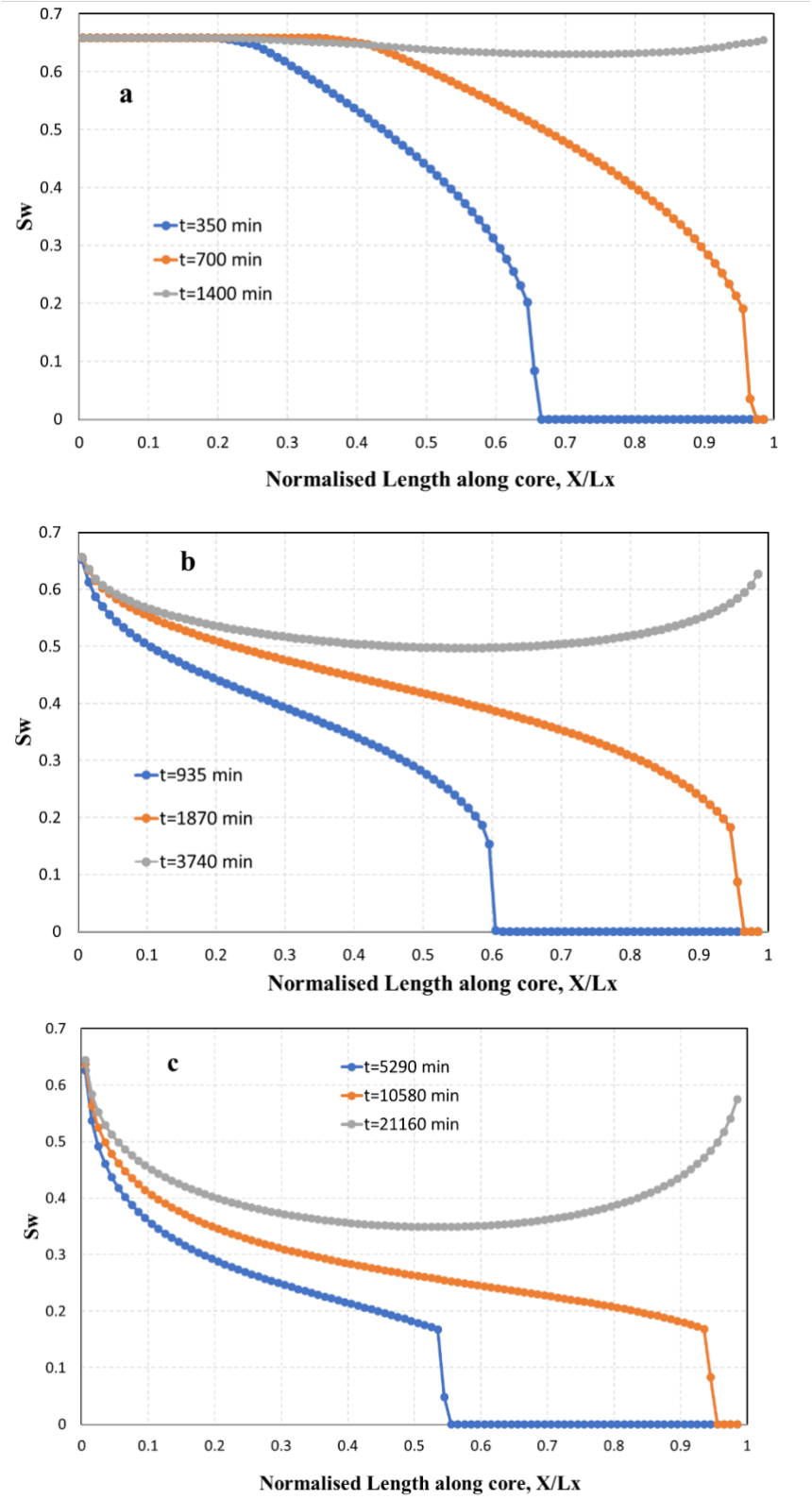

Figure 4.8: *Water saturation profile for CHP2 at fixed μ_w=1.09cP and varying μ_o=1cP (a), 32cP (b) and 1000cP (c). Each figure shows the saturation distribution at time equal to half BT (bottom, blue), at BT (middle, orange) and twice the BT (top, grey).*

4.2.2 Varying water viscosity at fixed oil viscosity

The impact of keeping the oil viscosity fixed while varying water viscosity was examined by running the model for CHP2 at water viscosities, μ_w*=1cP, 32cP and 1000cP.* The water viscosity was held constant at μ_o^{ref}*=1.09cP.* In Figure 4.10, results of the simulations conducted are presented as recovery factor versus time. This is recognized as an increase in the viscosity ratio, $\frac{\mu_o}{\mu_w}$.

The observed trends are similar, with increased imbibition time as water viscosity is increased. The breakthrough times occur at approximately 1000, 25000 and 800000 mins for the cases with relation to increasing water viscosities respectively. Through Figure 4.10 a-c, it is evident how that recovery by co-current imbibition gradually increases as μ_w is increased. It is also noticed that counter-current recovery reduces with increased water viscosity with almost zero counter-current RF at $\mu_w = 1000cP$ (COUCSI RF = 0.006, Figure 4.10c) and co-current recovery responsible for about 98% of the total recovery.

It is noteworthy that the behaviour of recovery by co-and counter -current imbibition are in converse when the system where oil viscosity is changed at fixed water viscosity is compared to the reverse system of increasing water viscosity at fixed oil viscosity. In the former (Figure 4.9 a1-c1), recovery by COCSI decreases while recovery by COUCSI increases whereas COCSI recovery increases while COUCSI decreases for the latter system (Figure 4.9 a2-c2).

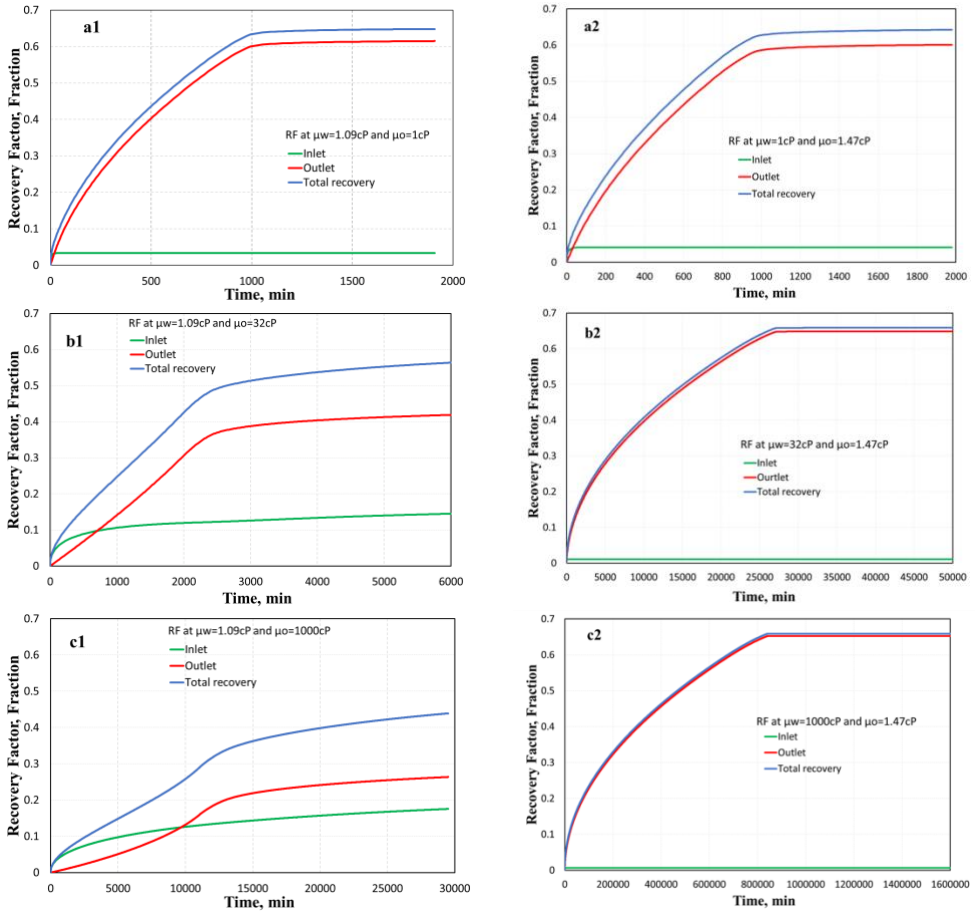

Figure 4.9: *Simulated RF versus time of CHP2 at fixed μ_w=1.09cP and varying μ_o=1cP (a1), 32cP (b1) and 1000cP (c1) compared to the system at fixed μ_o=1.47cP and varying μ_w=1cP (a2), 32cP (b2) and 1000cP (c2) . The figures show counter-current (inlet), co-current (outlet) and total recovery factor.*

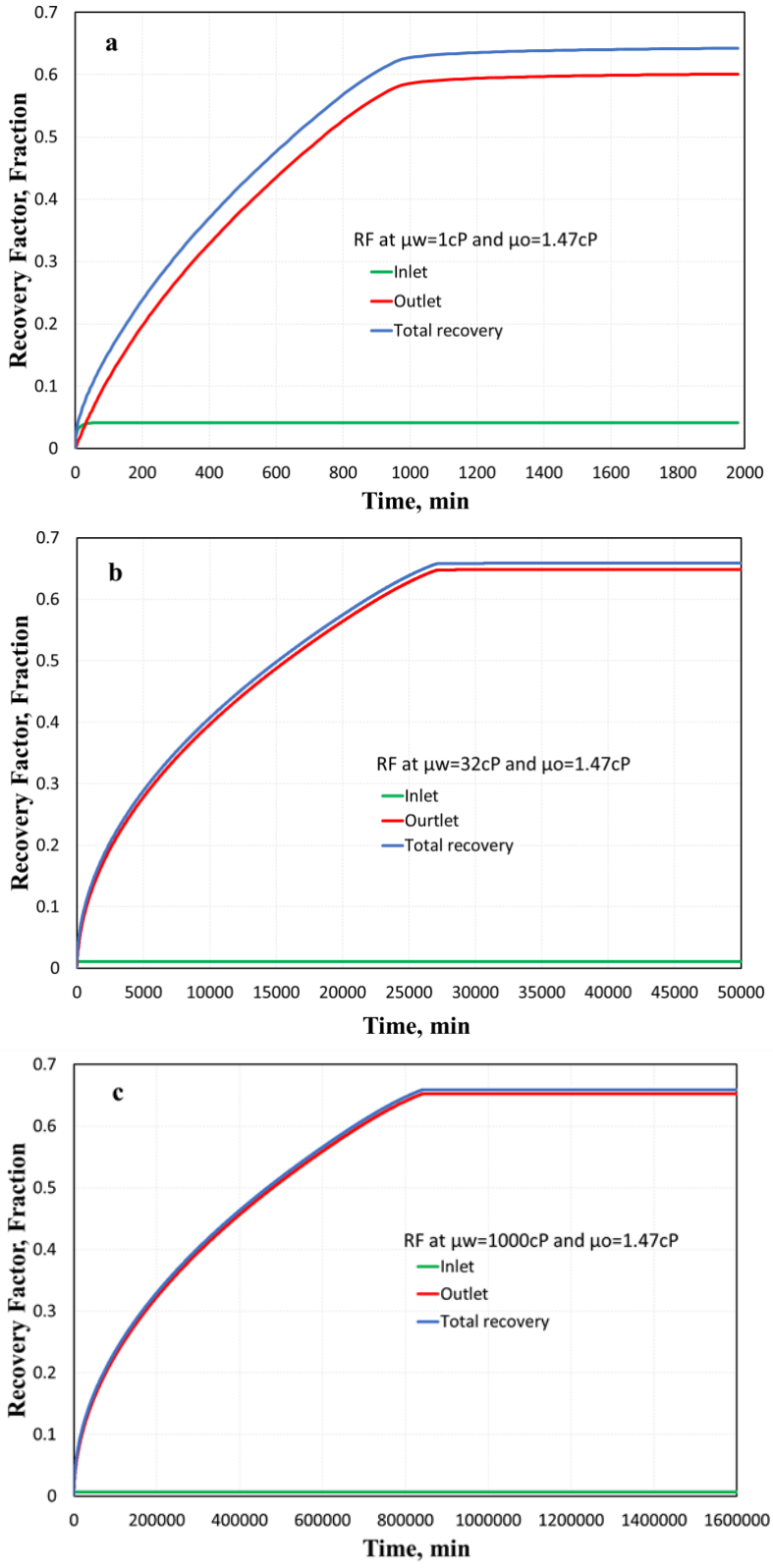

Figure 4.10: *Simulated RF versus time of CHP2 at fixed μ_o=1.47cP and varying μ_w=1cP (a), 32cP (b) and 1000cP (c). The figures show counter-current (inlet), co-current (outlet) and total (co- plus counter-current) recovery factor.*

4.2.3 Varying Viscosity at fixed mobility ratio

The initial Mobility Ratio of the experiment with CHP2 is M $= \left({k_{rw}^{max}}/{\mu_w}\right) / \left({k_{ro}^{max}}/{\mu_o}\right) \approx 0.2$. Figures 4.11 and Figures 4.12 presents analysis run for two cases: low mobility ratio (M << 1) and for a high mobility ratio (M >> 1). The desired mobility ratios achieved were $M \approx 0.01\left(20\mu_w^{ref}\right)$ and $M \approx 11\left(50\mu_o^{ref}\right)$ where the parenthesis indicates the applied increase of water or oil viscosity compared to the initial reference values.

In each case, the influence of increasing the viscosity ratio is investigated by increasing the water and oil viscosities by factors of three (3) and nine (9). It is observed by comparing the general trend in Figures 4.9, $M \approx 0.01\left(20\mu_w^{ref}\right)$, and Figures 4.11, ($M \approx 11\left(50\mu_o^{ref}\right)$, to that presented earlier in Figure 4.2 $M \approx 0.2\ (reference)$ that the imbibition rate is noticeably reduced in both cases where M is modified. At M = 0.01, water viscosity is increased, and the imbibing water will have low mobility. The total mobility of the system will therefore reduce as time progresses and this yields a decreased imbibition rate. In the other system, an increase in the oil viscosity (resulting in M = 11) lowers the oil mobility as compared to that of water and the reduced total mobility yields a decreased imbibition rate. However, the imbibition rate at M =11 is relatively higher than at M = 0.01. This can be attributed to the effect of increased water imbibition in the former system as compared to the latter. A similar observation has been reported in a simulation study by Andersen et al., (2018), where increasing the viscosity of water or oil from a reference case reduced the observed imbibition rate.

It is also observed that co-current recovery is reduced as the mobility ratio is increased from M = 0.01 (COCSI RF = 0.64) to M = 11 (COCSI RF = 0.40); whereas counter-current recovery is increased as the mobility ratio is increased from M = 0.01 (COCSI RF = 0.01) to M = 11 (COUCSI RF = 0.16). For the system at M = 0.01, the increased water viscosity reduced counter-current production, but did not have huge impact on the residual oil saturation when compared to the reference case (with RF = 0.60). Thus, the total amount of oil recovered remained nearly the same (Total RF for both = 0.65). This is consistent with the observations reported by Hamidpour et al., (2015) and Meng et al., (2017) on the influence that viscosity ratio increase at constant M has on the final recovery.

Considering plots a – c in Figures 4.10 and Figures 4.12, the same trend is observed respectively for the cases of increasing both water and oil viscosities by the same factor. It has been confirmed in a previous study by Fischer and Morrow, (2006) that increasing the viscosity ratio in this manner merely extends the overal imbibition time but has no influence on the recovery factor. The RF is principally controlled by M, and thus by increasing both phase viscosities by the same factor, M is constant except for the individual viscosities which increase and result in systematic reduction of the recovery rate. This phenomenon is well observed in the results presented in Figures 4.11 and Figures 4.12.

The saturation profile along the core for M = 0.01 and M = 11 are presented in Figure 4.13. The saturation distribution is plotted for the cases a – c at the same time, t = 1490. It is observed that the profile looks the same for each system of fixed M though the viscosities of water and oil are increasing (by the same factor). In essence, as peculiar to the Buckley-Leverett solution, the fronts are simply the same solutions but present at different positions. The smearing of the profile occurs as a result of capillary diffusion. It can be said, probably, that the only thing changing is the velocity of the front, as can be inferred from the slope of the profile. In the same BL-solution for each case, if the points of one profile plot was to be migrated to the position of the other by the same amount, a complete superposition will be obtained. Table 4.2 presents details on the modifications conducted on the viscosities as outlined her as well as the recovery values.

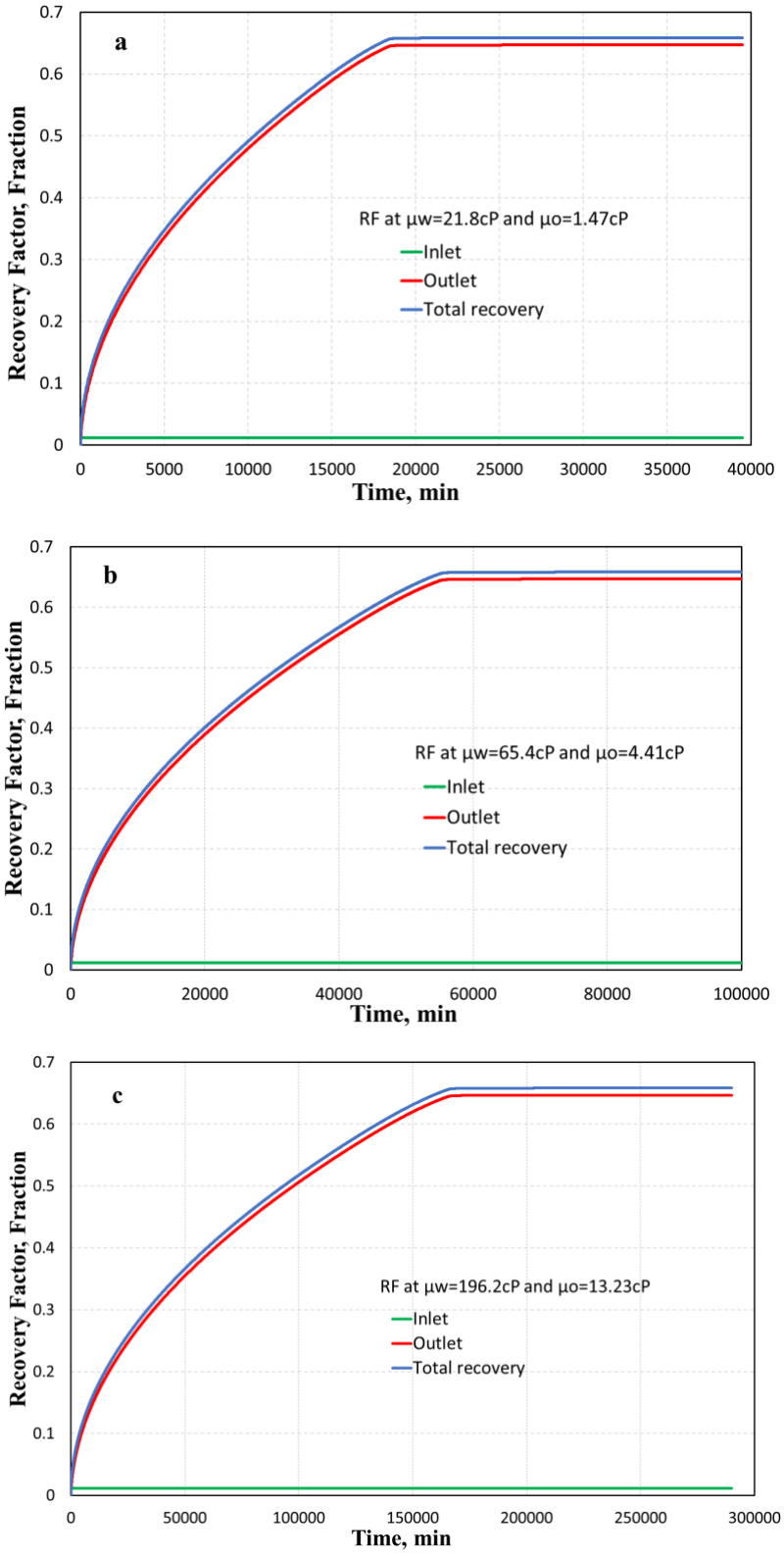

Figure 4.11: *Simulated RF versus time of CHP2 at fixed M=0.01 (a) but varying both μ_o and μ_w by the same factor of 3 (b) and 9 (c). The figures show counter-current (inlet), co-current (outlet) and total (co- plus counter- current) recovery factor.*

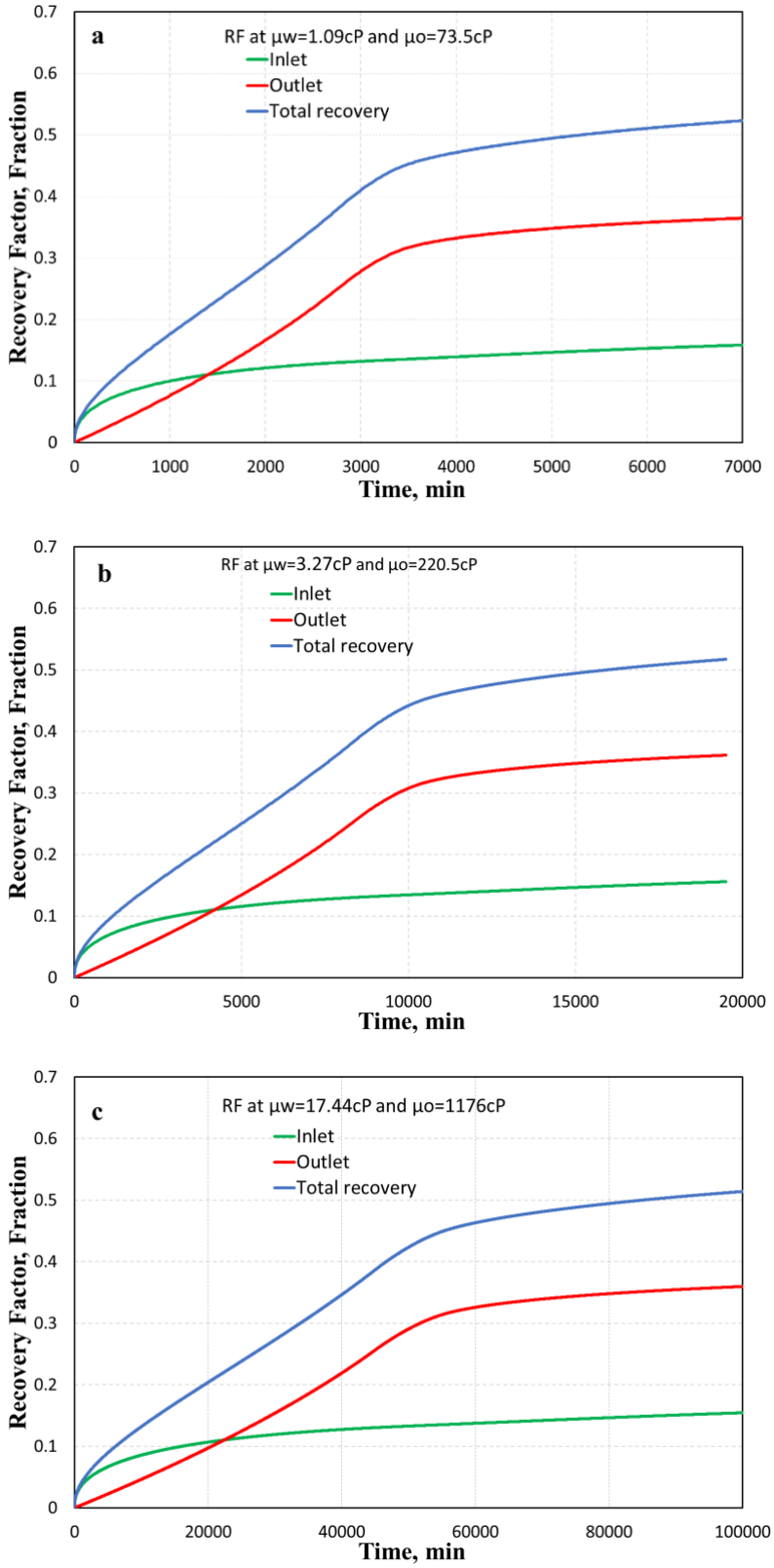

Figure 4.12: *Simulated RF versus time of CHP2 at fixed M=11 (a) but varying both μ_o and μ_w by the same factor of 3 (b) and 9 (c). The figures show counter-current (inlet), co-current (outlet) and total RF.*

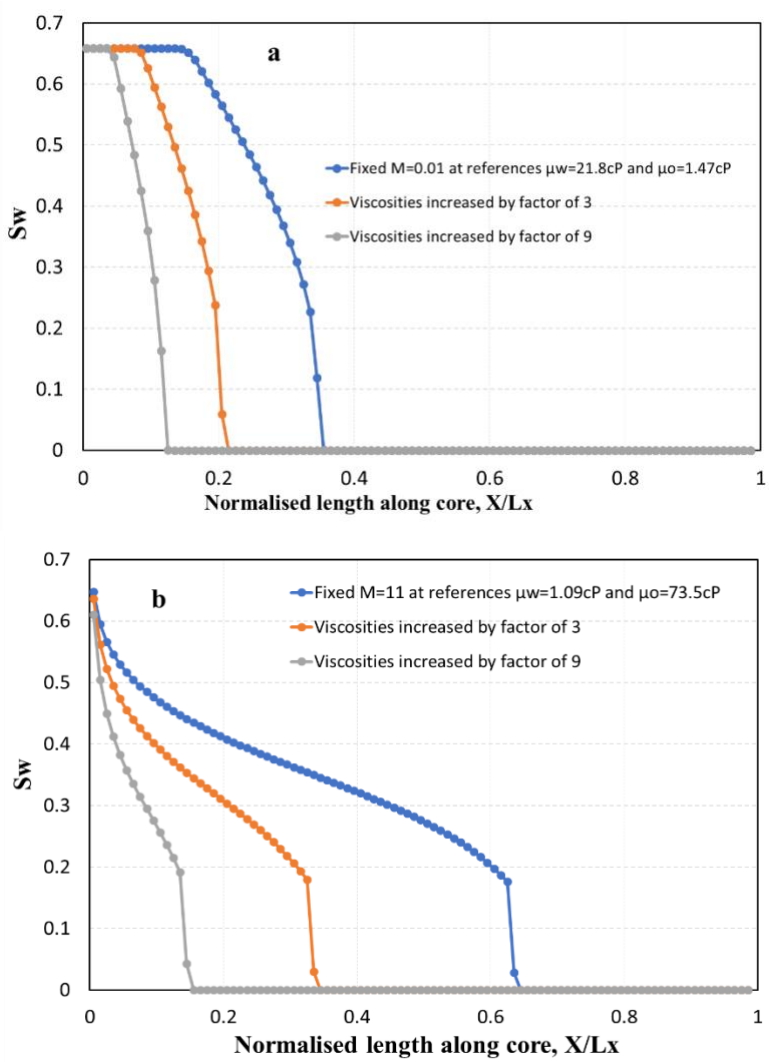

Figure 4.13: *Water saturation profile of CHP2 at fixed M=0.01 (a) and M =11 (b). Each figure shows the saturation distribution along the core at the same time, t=1490 for the systems representing the reference M (bottom, grey) and that obtained by varying both μ_o and μ_w by the same factor of 3 (middle, orange) and 9 (top, blue).*

Table 4.2: *Comparison of imbibition behaviour when μ_w and μ_o are increased by same scale (using factors 3 and 9) at fixed mobility ratio.*

	M=0.01		M=11	
	μ_w (cP)	μ_o (cP)	μ_w (cP)	μ_o (cP)
Reference	21.8	1.47	1.09	73.5
Case 1, (3*μ)	65.4	4.41	3.27	220.5
Case 2, (9*μ)	196.2	13.23	17.44	1176

4.2.4 Impact of capillary back pressure on imbibition recovery at M=0.01 and M=11

The cases at M = 0.01 and M = 11 were further studies to evaluate the influence of capillary back pressure (P_{cb}) on the recovery trend. The results are depicted in Figure 4.14. Originally, the model at these Mobility ratios are run at P_{cb} = 0 and then further explored with values of 0.15, 0.25 and 0.4 in dimensionless values. It is worthy of mention that the threshold capillary pressure used for the successful history match of the experimental data was ~0.09.

The behaviour of the system is more or less the same for M =0.01 (Figure 4.14 a1- d1) as compared to that at M =11 (Figure 4.14 a2- d2); in that counter current reduces as P_{cb} is increased and the imbibition time scales are constant throughout all four cases considered. However, the impact is minimal for M = 0.01 relative to M = 11.

In the system at $M \approx 11\left(50\mu_o^{ref}\right)$, the effect of P_{cb} is prominent. It is observed that increasing P_{cb} reduces the counter current recovery appreciably, with very little COUCSI production at P_{cb} = 0.4 (Figure 4.14 d2). Meng et al., (2015) reported low counter-current production in experimental TEOFSI studies, which was attributed to the presence of a semi-permeable filter at the inlet side that increased the capillary back pressure.

The nature of imbibition recovery by co- and counter- current imbibition are separately presented in Figure 4.15 as well as the total recovery factor. It is interesting to observe that the recovery curves at P_{cb} = 0 and 0.15 nearly overlap. The co-current recovery curves (Figure 4.15b) for all cases are linear and overlap until after t =1500, where the curves become easily distinguishable with the imbibition rate seen to decrease with increased P_{cb} and a final co-current RF that is higher at higher P_{cb} values. Breakthrough is also observed to be delayed when P_{cb} is increased.

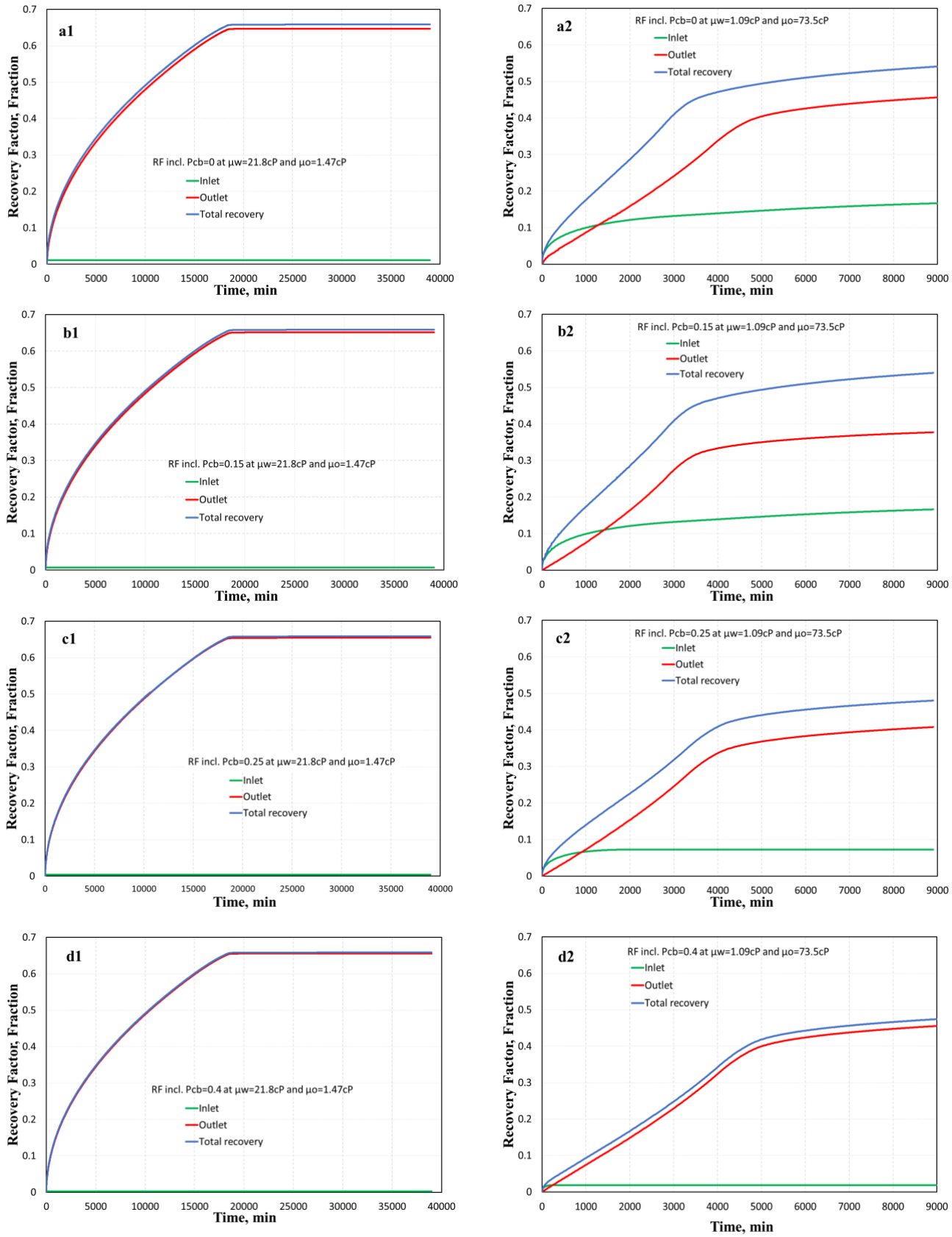

Figure 4.14: *Simulated RF versus time of CHP2 at fixed M=0.01 (left, index 1) & M=11(right, index 2) by using P_{cb} values 0 (a), 0.15(b),0.25(c) and 0.4(d). The figures show counter-current (inlet), co-current (outlet) and total RF.*

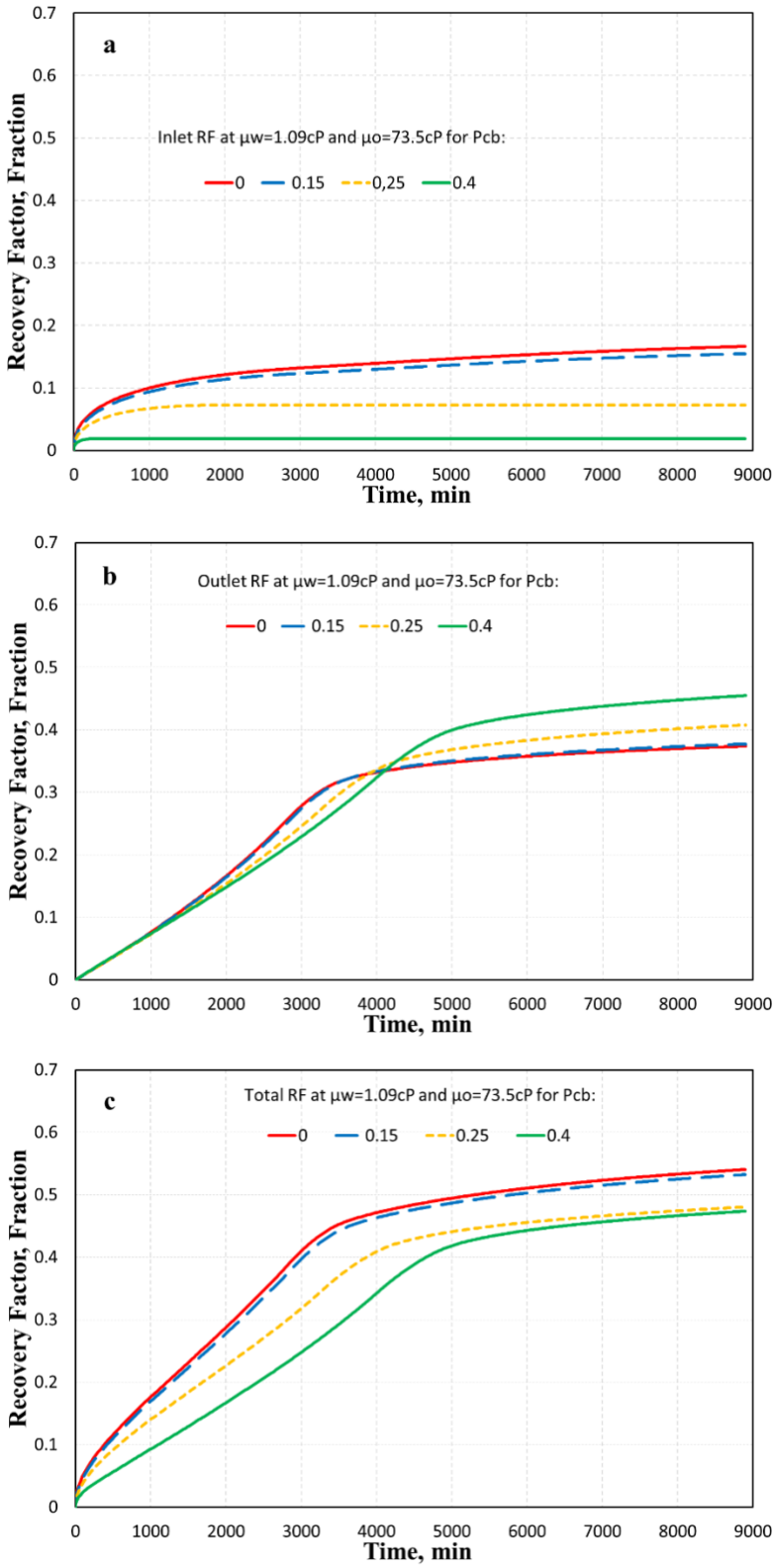

Figure 4.15: *Simulated RF versus time of CHP2 at fixed M=11 and using P_{cb} values 0 (a), 0.15(b), 0.25(c) and 0.4(d) The figures show counter-current (inlet-a), co-current (outlet-b) and total RF.*

5 CONCLUSIONS AND FURTHER STUDIES

The simulation study was aimed at investigating the influence of certain key parameters on co-, counter- and total oil recovery under experimental conditions employing the Two-Ends-Open Free Spontaneous Imbibition boundary condition.

Based on this study the following conclusions can be made:

- Imbibition of water into a core originally filled with oil exhibits co-current production at the side exposed to oil and counter-current production at the side exposed to water in a manner. The boundary condition is more favourable for co-current production.

- The experimental data was matched satisfactorily using saturation functions obtained by manual history matching and employing a one-dimensional numerical model with the IORCoreSim.

- When the oil viscosity is increased at a fixed water viscosity, imbibition rate is lower with decreasing co-current production whereas counter-current recovery is increased. The breakthrough time was observed to be delayed during such evaluation.

- When water viscosity is increased at fixed oil viscosity, the individually observed trends for co- and counter-current recovery are similar with increased imbibition time noticed as well. The breakthrough time is also observed to be delayed during such evaluation.

- The viscosity ratio is scaled by a factor of 3 and 9 at fixed mobility ratios of M = 0.01 and M =11. Higher imbibition rates are attained for M=11 as compared to M=0.01. The general trend moreover shows that increasing viscosity ratio does not influence the total production. It was noted that co-current recovery reduces as M increases from 0.01 to 11 whereas counter-current production increased. The saturation profile along the core exhibited similar trend for the cases examined.

- The impact of Capillary Back Pressure (CBP) on imbibition recovery at fixed M=0.01 and M=11 was studied. It is observed that the CBP exercises a huge impact on the system at M=11 compared to M=0.01. The general observed trend was a reduced counter-current recovery as the CBC was increased at magnitudes beyond the threshold capillary pressure.

The following are suggested for further studies:

- Further sensitivity analysis can be performed that investigates the influence of the shape of the saturation functions on the imbibition recovery using TEOFSI boundary conditions.

6 REFERENCES

Abdallah, W., Buckley, J., Carnegie, A., Fordham, E., Edwards, J., Herold, B., . . . Ziauddin, M. (2007). *Fundamentals of Wettability.* Alberta, Canada: OilField review.

Akin, S., Schembre, J., & Kovscek, A. (1998, May). Spontaneous Water Imbibition into Diatomite. 1-11.

Andersen, P., Brattekås, B., Oddbjørn, N., Lohne, A., Føyen, T., & Fernø, M. (2018a). Darcy Scale Simulation of Boundary Condition Effects during Capillary Dominated Flow in High Permeability Systems. *SPE Reservoir Evaluation and Eng.*

Andersen, P., Brattekås, B., Walrond, K., Aisyah, D., Nødland, O., Lohne, A., . . . Fernø, M. (2017). Numerical Interpretation of Laboratory Spontaneous Imbibition - Incorporation of the Capillary Back Pressure and How it Affects SCAL. *Abu Dhabi International Petroleum Exhibition & Conference.* Abu Dhabi: SPE.

Andersen, P., Evje, S., & Hiorth, A. (2017). Modeling of Spontaneous-Imbibition Experiments With Porous Disk—On the Validity of Exponential Prediction. *SPE Journal, 22*(05). doi:https://doi-org.ezproxy.uis.no/10.2118/186094-PA

Andersen, P., Evje, S., & Kleppe, S. (2013). A Model for Spontaneous Imbibition as a Mechanism for Oil Recovery in Fractured Reservoirs. *Transport in porous media, 101*(02), 299-331.

Andersen, P., Lohne, A., Stavland, A., Hiorth, A., & Brattekås, B. (2018b). Core Scale Simulation of Spontaneous Solvent Imbibition from HPAM Gel. *SPE Improved Oil Recovery Conference.* Tulsa, Oklahoma, USA: SPE.

Andersen, P., Qiao, Y., Standnes, D., & Evje, S. (2018). Co-Current Spontaneous Imbibition in Porous Media with the Dynamics of Viscous Coupling and Capillary Back Pressure. *SPE Improved Oil Recovery Conference.* Tulsa, Oklahoma, USA: SPE. Retrieved from https://doi.org/10.2118/190267-MS

Andersen, P., Skjæveland, S., & Standnes, D. (2017). A novel bounded capillary pressure correlation with application to both mixed and strongly wetted porous media. *SPE Abu Dhabi international petroleum exhibition and conference.* Abu Dhabi, UAE: SPE.

Anderson, W. G. (1986). Wettability Literatur Survey-Part1: rock/oil/brine iteractions and the effects of core handling on wettability. *Journal of Petroleum Technology, 38*, 1125-1144.

Anderson, W. G. (1987). Wettability Literature Survey-Part 6: The Effects of Wettability on Waterflooding. *JPT, 39*(12), 1605-1622.

Austad, T., & Milter, J. (1997). Spontaneous Imbibition of Water Into Low Permeable Chalk at Different Wettabilities Using Surfactants. *International Symposium on Oilfield Chemistry.* Houston: SPE.

Austad, T., Matre, B., & Milter, J. (1998). Chemical flooding of oil reservoirs 8. Spontaneous oil expulsion from oil-and water-wet low permeable chalk material by imbibition of aqueous surfactant solutions. *Colloids Surf., 137*(1-3), 117-129.

Babchin, A., Yuan, J., & Nasr, T. (1998). Generalized phase mobilities in gravity drainage processes. *Paper presented at the Annual Technical Meeting,*. Calgary, Alberta.

Baker, A. (1988). Three-Phase Relative Permeability Correlations. *SPE Enhanced Oil Recovery Symposium* (pp. 539-554). Tulsa, Oklahoma: SPE.

Bear, J., & Verruiit, A. (1987). Theory and applications of transport in porous media. In J. Crolet (Ed.), *Modeling of groundwater flow and pollution,* (Vol. 17). Dordrecht: Reidel.

Bentsen, R., & Anli, J. (1977, February). Using parameter estimation techniques to convert centrifuge data into a capillary-pressure curve. *SPE J., 17*(01), 57-64.

Bourbiaux, B. (2009). Understanding the oil recovery challenge of water drive in fractured reservoirs. *The International Petroleum Technology Conference.* Doha, Qatar.

Bourbiaux, B. J. (1990, August). Experimental Study of Cocurrent and Countercurrent Flows in Natural Porous Media. *SPE Reservoir Engineering, 5*(03).

Brooks, R., & Corey, A. (1964). Hydraulic properties of porous media. *Hydrology Papers, 3*.

Brownscombe, E., & Dyes, A. (1952). Water-imbibition Displacement-A Possibility for the Spraberry. *Drilling and Production Practice, 1 January, New York, New York.* New York: American Petroleum Institute.

Buckley, S., & Leverett , M. (1942). Mechanism of fluid displacement in sands. *Trans. AIME, 146*(01), 107-116. Retrieved from https://doi-org.ezproxy.uis.no/10.2118/942107-G

Cai, J., Yu, B., & Zou, M. (2010). Fractal characterization of spontaneous co-current imbibition in porous media. *Energy Fuels, 24*(03), 1860-1867.

Chen, H., Lucas, L., Nogaret, L., Yang, H., & Kenyon, D. (2000). Laboratory Monitoring of Surfactant Imbibition Using Computerized Tomography. *SPE International Petroleum Conference and Exhibition in.* Mexico, Villahermosa, Mexico.

Chen, Z., Huan, G., & Ma, Y. (2006). *Computational methods for multi-phase flows in porous media* (Vol. 2). Philadelphia: SIAM.

Chilingar, G. V., & Yen, T. F. (1983). Some Notes on Wettability and Relative Permeabilities of Carbonate Reservoir Rocks, II. *Energy sources, 7*(01), 67-75.

Corey, A. (1954). The interrelation between gas and oil relative permeabilities. *Producers monthly, 19*(01), 38-41.

Craig, F. (1971). The reservoir engineering aspects of waterflooding. Dallas, Texas, US.

Cuiec, L. (1991). Evaluation of reservoir wettability and its effect. In *N.R.Interfacial Phenomena in Oil Recovery by Norman R. Morrow* (pp. 319-375). New York: Marcel Decker.

Cuiec, L., Bourbiax, B., & Kalaydjian, E. (1994). Oil recovery by imbibtion in low permeability chalk. *SPE Formation Evaluation, 9*(3).

Donaldson, E., & Waqi, A. (2008). *Wettability.* Houston, Texas: Gulf Publishing Company.

Fernø, M., Haugen, Å., Mason, G., & Morrow, N. (2014). Measurement of Core Properties Using a New Technique Two Ends Open Spontaneous Imbibition. *International Symposium of the Society of Core Analysts*, (pp. 8-11). Avignon, France.

Fischer, H., & Morrow, N. (2006). Scaling of oil recovery by spontaneous imbibition for wide variation in aqueous phase viscosity with glycerol as the viscosifying agent. *J. of Pet. Sxci. and Eng., 52*(01-04), 35-53.

Foley, A., Nooruddin, H., & Blunt, M. (2017). The impact of capillary backpressure on spontaneous counter-current imbibition inporous media. *Advances in Water Resources, 107*, 405-420. Retrieved from https://doi.org/10.1016/j.advwatres.2017.04.012

Frida, Y. (1998). *A study of imbibition mechanisms in the naturally fractured Spraberry Trend area.* PhD Thesis, New Mexico Institute of Mining and Technology, Dept. of PEtroleum and Natural Gases, New Mexico.

Gupta, R., & Mohanty, K. (2010). Temperature effects on surfactant-aided imbibition into fractured carbonates. *SPE J., 15*(03), 588-597.

Hamidpour, E., Mirzaei-Paiaman, A., Masihi, M., & Harimi, B. (2015, October 9). Experimental study of some important factors on nonwetting phase recovery by cocurrent spontaneous imbibition. *Journal of Natural Gas Science and Engineering, 27*, 1213-1228.

Handy, L. (1960). Determination of Effective Capillary Pressures for Porous Media from Imbibition Data. *Petroleum Transactions, AIME, 219*, 78-80.

Hatiboglu, C., & Babadagli, T. (2010). Experimental and visual analysis of co- and counter-current spontaneous imbibition for different viscosity ratios, interfacial tensions, and wettabilities. *Journal of Petroleum Science and Engineering, 70*(3-4), 214-228.

Haugen, Å., Fernø, M., Mason, G., & Morrow, N. (2014). Capillary pressure and relative permeability estimated from a single spontaneous imbibition test. *J. of Pet. Sci. and Eng., 115*, 66-77.

Haugen, Å., Fernø, M., Mason, G., & Morrow, N. (2015, January). The Effect of Viscosity on Relative Permeabilities Derived from Spontaneous Imbibition. *Transport in Porous Media, 106*, 383-404.

Karimaie, H., Torsæter, O., Esfahani, M., Dadashpour, M., & Hashemi, S. (2006). Experimental investigation of oil recovery during water imbibition. *J. of Pet. Sci. and Eng., 52*(1-4), 297-304.

Karpyn, Z., Halleck, P., & Grader, A. (2009). An experimental study of spontaneous imbibition in fractured sandstone with contrasting sedimentary layers. *J. Petrol. Sci. Eng, 67*(1-2), 48-56.

Kleppe, J. (2014). *Review of relative permeabiltiy and capillary pressures.* NTNU, Dept. of Geoscience and Petroleum, Trondheim. Retrieved from http://www.ipt.ntnu.no/~kleppe/TPG4150/krpc.pdf

Leverett , M. (1929). *Trans AIME, 132*, 151-169.

Leverett, M. (1941). Capillary Behavior in Porous Solids. *Capillary Behavior in Porous Solids*.

Li, K. (2007). Scaling of spontaneous imbibition data with wettability included. *Journal of Contaminant Hydrology, 89*(3-4), 218-230.

Li, K., & Horne, R. (2006, January). Generalized Scaling Approach for Spontaneous Imbibition: An Analytical Model. *SPE Reservoir Evaluation & Engineering*, *9*(03).

Li, Y., Morrow, N., & Ruth, D. (2003). Similarity solution for linear counter-current spontaneous imbibition. *J. Pet. Sci. Eng., 39*(03-04), 309-326.

Lohne, A. (2017). *User manual for IORCoreSIm-combined EOR and SCAL sumulator*. Stavanger, Norway: IRIS.

Lomeland, F., Ebeltoft, E., & Hammervold, T. (2008). A new versatile capillary pressure correlation. *Symposium of the society of core analysts. 29.* Abu Dhabi, UAE: SPE.

Ma, S., Morrow, N., & Zhang, X. (1997). Generalized Scaling of Spontaneous Imbibition Data for Strongly Water-Wet Systems. *J. Pet. Sci. and Eng., 18*, 165-178.

Ma, S., Morrow, N., & Zhang, X. (1999). Influence of fluid viscosity on mass transfer between rock matrix and fractures. *Journal of Canadian Petroleum Tchnology, 38(07)*.

Mason, G., & Morrow, N. (2013, October). Developments in spontaneous imbibition and possibilities for future work. *J. of Pet. Sci. and Eng., 110*, 263-293.

Mason, G., Fischer, H., Morrow, N., & Ruth, D. (2009, June). Spontaneous Counter-Current Imbibition into Core Samples with All Faces Open. *Transport in porous media, 78*(02), 199-216.

Mason, G., Fischer, H., Morrow, N., & Ruth, D. (2010). Correlation for the Effect of Fluid Viscosities on Counter-current Spontaneous Imbibition. *J. of Pet. Sci. and Eng., 27*(1-2), 195-205.

Mason, G., Fischer, H., Morrow, N., Johannesen, E., Haugen, Å., & Graue, A. F. (2010, January 10). Oil Production by Spontaneous Imbibition from Sandstone and Chalk Cylindrical Cores with Two Ends Open. *Energy Fuels, 24*(02), 1164-1169.

Mattax, C., & Kyte, J. (1962). Imbibition Oil Recovery from Fractured, Water-Drive Reservoir. *SPE J, 2*(02), 177-184.

McCardell, W. (1955). A Review of the Physical Basis for the Use of the J-Function. *Eighth Oil Recovery Conference.* Texas Petroleum Research Committee.

McWhorter, D., & Sunada, D. (1990). Exact integral solutions for two-phase flow. *Water Resour., 26*(03).

Meng, Q., Liu, H., & Wang, J. (2015). Entrapment of the Non-wetting Phase during Co-current Spontaneous Imbibition. *Energy fuels, 29*, 686-694.

Meng, Q., Liu, H., & Wang, J. (2017). A critical review on fundamental mechanisms of spontaneous imbibition and the impact of boundary condition, fluid viscosity and wettability. *Advances in Geo-Energy Research, 1*(1), 1-17.

Meng, Q., Liu, H., & Wang, J. (2017, May). Effect of viscosity on oil production by cocurrent and countercurrent imbibition from cores with two ends open. *Reservoir |Evluation and Engineering*, 251-259.

Meng, Q., Liu, H., Wang, J., & Zhang, H. (2016). Effect of Wetting-Phase Viscosity on Cocurrent Spontaneous Imbibition. *Energy Fuels, 30*, 835-843.

Morrow, N., & Mason, G. (2001). Recovery of oil by spontaneous imbibition. *6*(04).

Muskat, M. (1946). Flow of homogeneous fluids through porous media. *No. 532.5 M88*.

Neshat, S., & Pope, G. (2017). Compositional Three-Phase Relative Permeability and Capillary Pressure Models Using Gibbs Free Energy. *SPE Reservoir Simulation Conference.* Montgomery, Texas, USA: SPE.

O'Carrol, D., Abriola, L., Polityka, C., Bradford, S., & Demond, A. (2005, May). Prediction of two-phase capillary pressure–saturation relationships in fractional wettability systems. *J. of Contaminant Hydrology, 77*(4).

Pooladi-Darvish, M., & Firoozabadi, A. (2000). Cocurrent and countercurrent current imbibition in a water-wet matrix block. *SPE J, 5*(01), 3-11.

Puntervold, T., Shariatpahani, S., Hopinks, P., Aksulu, S., Austad, T., & Strand, S. (2016). Water Based EOR by Wettability Alteration in Dolomite,. *Energy and Fuels, 30*(01), 180-187.

Qasem, F., Nashawi, I., Gharbi, R., & Mir, M. (2008). Recovery performance of partially fractured reservoirs by capillary imbibition. *Journal of Pet. Sci. and Tech., 60*(01), 39-50.

Rao, D. R. (1996). "Wettability Effects in Thermal Recovery Operations. *SPE/DOE IMproved OIl Recovery Symposium.* Tulsa: SPE.

Rose, W. (1988). Measuring transport coefficients necessary for the description of coupled two-phase flow of immiscible fluids in porous media. *Transport in Porous Media,, 3*(02), 163-171.

Salathiel, R. A. (1973). Oil recovery by surface film drainage in mixed wettability rocks. *JPT, 25*(10), 1216-1224.

Schechter, D., Zhou, D., & Orr, F. (1994). Low IFT drainage and imbibition. *J. Pet. Sci and Eng., 11*(04), 283-300.

Schmid, K., & Geiger, S. (2011). Universal scaling of spontaneous imbibition for water-wet systems. *Water Resour., 48*(03).

Siddiqui, S., Yang, J., & Ahmed, M. (1988). Dynamic displacement measurement of three-phase relative permeabilities in Berea sandstone cores. *SPE Annual Technical Conference and Exhibition* (pp. 759-767). New Orleans, Louisiana: SPE.

Skjæveland, S., Siqveland, L., & Kjosavik, A. (2000). Capillary pressure correlation for mixed+wet reservoirs. *SPE Res. Eval. and Eng., 3*(01), 60-67.

Standnes, D. (2004). Experimental study of the impact of boundary conditions on oil recovery by co-current and counter-current spontaneous imbibition. *Energy Fuels, 18*(01), 271-282.

Standnes, D., & Andersen, P. (2017). Analysis of the Impact of Fluid Viscosities on the Rate of Countercurrent Spontaneous Imbibition. *Energy & Fuels, 31*(07), 6928-6940.

Strand, S., Puntervold, T., & Austad, T. (2007). "Water Flooding of Carbonate Reservoirs: Effects of a Model Base and Natural Crude Oil Bases on Chalk Wettability,. *Energy and Fuels, 21*(03), 1606-1616.

Szymkiewicz, A. (2012). Modelling water flow in unsaturated porous media: accounting for nonlinear permeability and material heterogeneit. Berlin, Germany: Springer Science & Business Media.

Tarek, A. (2006). Fundamentals of rock properties. In *Reservoir Engineering Handbook* (Vol. 3). Elsevier.

Torsæter, O., & Abtahi, M. (2003). *Experimental reservoir engineering laboratory work book.* Trondheim, Norway: NTNU.

Treiber, L., Archer, D., & Owens, W. (1972). A Laboratory Evaluation of the Wettability of Fifty Oil-Producing Reservoirs. *SPE J., 12*(06), 531-546.

Unsal, E., Mason, G., Morrow, N., & Ruth, D. (2009). Bubble snap-off and capillary-back pressure during counter-current spontaneous imbibition into model pores. *Langmuir, 25*(06), 3387-3395.

Wade, W. (1974, April). Spontaneous Imbibition of Fluids in Porous Vycor. *14*(02).

Watts, J. (1986). A compositional formulation of the pressure and saturation equations. *SPE Res. Eng., 1*(03), 243-252.

Yoldiz, H., Gokmen, M., & Cesur, Y. (2006). Effect of shape factor, characteristic length, and boundary conditions on spontaneous imbibition. *J. Pet. Sci. Eng., 53*(03-04), 158-170.

Zhou, X., Morrow, N., & Ma, S. (2000). Interrelationship of Wettability, Initial Water Saturation, Aging Time, and Oil Recovery by Spontaneous Imbibition and Waterflooding. *SPE Journal, 5*(00), 199-207.

7 APPENDIX

7.1 A1 – Input for Saturation Functions

Summary of Input for Simulator			
Sw	Krw	Kro	J
0.0000	0	1.000E+00	0.802395
0.04	2.08983E-07	9.731E-01	0.800291
0.08	8.43373E-06	0.9383246	0.798187
0.0943	2.03793E-05	0.923998	0.796084
0.1088	4.3878E-05	0.9084499	0.79398
0.1233	8.5692E-05	0.8918802	0.791876
0.1378	0.000155007	0.8742987	0.789773
0.1523	0.00026355	0.8557184	0.787669
0.1668	0.000425738	0.8361558	0.787038
0.1813	0.000658724	0.815631	0.716776
0.1958	0.000982345	0.7941679	0.657099
0.2103	0.001418958	0.7717942	0.605718
0.2248	0.001993181	0.7485415	0.560967
0.2393	0.002731522	0.7244456	0.521605
0.2538	0.003661934	0.6995468	0.486685
0.2683	0.004813286	0.6738895	0.455474
0.2828	0.006214781	0.6475228	0.427392
0.2973	0.007895325	0.6205002	0.401978
0.3118	0.009882877	0.5928801	0.378857
0.3263	0.012203797	0.5647257	0.357723
0.3408	0.014882196	0.536105	0.338322
0.3553	0.017939331	0.5070912	0.320442
0.3698	0.021393029	0.4777622	0.303906
0.3843	0.025257188	0.4482012	0.288563
0.3988	0.029541337	4.185E-01	0.274284
0.4133	0.034250283	0.3887421	0.260959
0.4278	0.039383848	0.3590364	0.248492
0.4423	0.044936694	0.3294838	0.2368
0.4568	0.050898248	0.300194	0.225811
0.4713	0.057252721	0.2712824	0.215461
0.4858	0.063979215	0.24287	0.205694
0.5003	0.071051927	0.2150839	0.196461
0.5148	0.078440422	0.1880579	0.187717
0.5293	0.086109994	0.1619326	0.179423
0.5438	0.094022082	1.369E-01	0.171545
0.5583	0.102134743	0.1129903	0.164051
0.5728	0.110403173	0.0905034	0.156912
0.5873	0.118780259	6.959E-02	0.150102
0.6018	0.127217155	0.0504501	0.1436
0.6128	0.133626818	0.037279	0.138859
0.6238	0.140020075	0.0254221	0.134274
0.6358	0.146949859	0.0142123	0.129441
0.6478	0.153805274	0.0052087	0.124774
0.6588	0.16	0	0.113257
0.6698	0.166087269	0	0.092141
0.672	0.167289991	0	0